NSLS II TECHNICAL NOTE BROOKHAVEN NATIONAL LABORATORY	NUMBER **NSLSII-ASD-TN-061**
AUTHOR T. Shaftan R. Fliller, R. Heese, J. Skaritka, J. Rose, S. Sharma, G. Ganetis, B. Dalesio, and D. Hseuh	DATE Rev.2 11/16/2009
TITLE **NSLS-II Booster Design**	

Introduction

The NSLS-II booster is required to produce a 3 GeV bunch train with an accelerated charge of about 10 nC at a repetition rate of 1 Hz and a horizontal beam emittance around 40 nm-rad. Injection into the booster ring takes place at an energy of 200 MeV. The booster magnetic field and RF voltage are ramped for 500 ms to accelerate the electron beam from the injection energy to the nominal energy of 3 GeV. At the maximum field of the ramp, the electron beam is extracted from the booster and injected into the Storage Ring. We allow for a maximum beam loss of 30% during injection, 20% maximum loss during extraction. Thus the charge to be accelerated in the booster is 10 nC which corresponds to an average beam current of 20 mA.

Since the dynamic aperture of the storage ring is limited, the quality of the injected beam has received serious consideration. In particular, the booster emittance may impact the injection efficiency. As the beam intensity in the storage ring is intended to be quasi-constant by frequently (once per minute) injecting beam into the storage ring (top-off injection) good injection efficiency is mandatory to minimize the frequency of top-off cycles, radiation dose induced by the lost electrons and perturbations of the stored beam orbit driven by the injection transients.

During the last 10 years, many 3rd generation synchrotron light facilities have been put into operation. Nearly all of these facilities have chosen a full energy booster synchrotron as an injector together with a low energy linac as pre-injector. The main parameters of several modern booster synchrotrons are listed in Table 1.

Table 1: Modern Boosters.

	ASP [1]	DIAMOND [2]	SOLEIL [3]	SLS [4]	ALBA [5]	BINP [6]
Energy, GeV	3	3	2.75	2.4	3	2.5
Tunnel	separate	separate	separate	same	same	separate
Circumference, m	130.2	157	157	270	249.6	132
Lattice	4-fold	2-fold	2-fold	3-fold	4-fold	2-fold
Rep rate, Hz	1	5	3	3	3	1
Emittance, nm	34	144	150	9	9	50
Tunes, X/Y	9.2/3.3	6.8/4.6	6.4/4.4	12.4/8.4	12.4/7.4	9.1/9.1
Chromaticity, X/Y	-8.8/-11.5	-8.4/-6.2		-15/-12	-17/-10	-11.6/-11.4
RF freq., MHz	500	500	352	500	500	181
Damping times, X/Y/E	2.7/3.5/2.0	5.4/5.5/2.7	6.3/5.7/2.7	11/19/14	4.5/8.0/1.8	4.4/4.2/2.1
Current, mA	7	20	15	1	5	50

Booster-synchrotrons for synchrotron light sources with energies around 3 GeV have natural horizontal emittances of the extracted beam in the 10–150 nm range. For example DIAMOND [2] and SOLEIL [3] boosters (located in separate buildings) have emittance of 140 nm; SLS [4] and ALBA [5] boosters (located in the ring tunnel) have emittances of 9 nm. The recently commissioned booster for the Australian light source (Australian

Synchrotron Project or ASP [1]) with a circumference of 130.2 m has an emittance of 34 nm. The relatively low ASP booster emittance in combination with rather small circumference and the choice of a combined-function FODO lattice looks attractive as it constitutes an existing, proven design which meets the NSLS-II design requirements. A series of injection tracking simulations for the storage ring [7] convincingly demonstrated that a booster emittance in the range of 30-50 nm would satisfy the demands for low-loss injection into the storage ring taking into account the necessary margins for injection errors. For this reason, the ASP booster has been chosen as a model for the NSLS-II booster development. However, there are a few major differences between the NSLS-II and the ASP design:

- The NSLS-II booster injection energy is 200 MeV (in contrast with 100 MeV at ASP)
- The nominal dipole field at 3 GeV is chosen to be 1.1 T (in contrast to 1.25 T at ASP)
- The NSLS-II booster circumference is 158.4 m (one-fifth of the storage ring circumference)
- Straight section length is 8.6 m, compared with 5.25 m at ASP
- The NSLS-II booster current is expected to be 20 mA (in contrast to 5 mA at ASP)

The RF frequency of the NSLS-II booster is chosen as 500 MHz. The booster revolution period of 528 ns restricts the length of the injected bunch train to be shorter than about 300 ns taking into account the finite rise- and fall-time of the injection and extraction kickers. Therefore the longest bunch train generated by the linac will consist of 150 bunches separated by 2 ns. The minimum bunch train length is 80 bunches, limited by the beam loading in the linac.

One of the important requirements for the NSLS-II booster is high efficiency of the charge transport through the booster. Therefore a careful job must be done for optimization of the booster injection and extraction, expansion of booster magnet tolerances, design of robust orbit correction system and maximization of dynamic aperture. In the next section, the NSLS-II booster model is discussed in detail.

1. Booster lattice

Every superperiod in the four-fold symmetric lattice is designed with five identical cells together with two modified cells containing dispersion suppressors. This results in a sufficiently low horizontal emittance of 40 nm-rad at the extraction energy of 3.0 GeV. The booster lattice structure and the linear lattice functions are depicted in Figure 1.

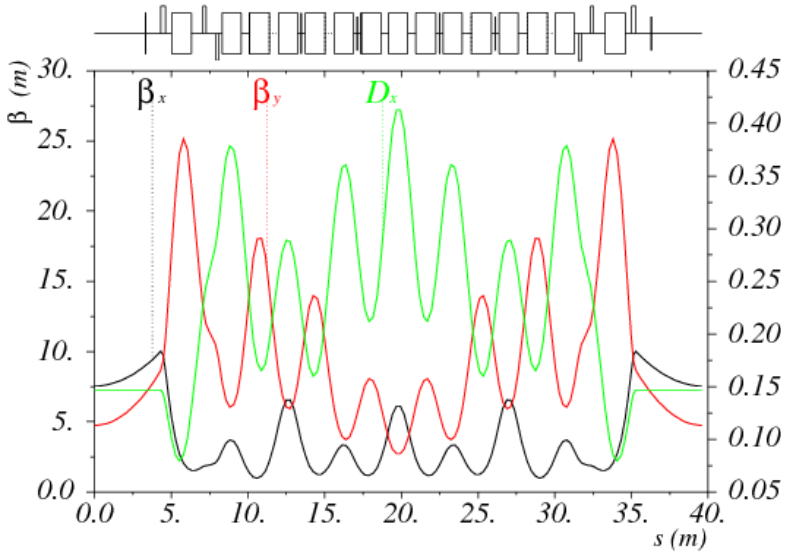

Figure 1: Twiss functions of one-quarter of the NSLS-II booster lattice. Black, red and green curves correspond to the horizontal and vertical beta-functions and the dispersion respectively.

The lattice contains four long (8.62 m) straight sections with low dispersion (less than 15 cm), long enough for the installation of RF cavities, injection and extraction systems, and diagnostics. The low-emittance lattice design requires strong focusing which results in a fairly large natural chromaticity (horizontal: -9.9, vertical -12.9). The peak value of the dispersion is quite low. This is the reason to integrate the sextupoles for the chromaticity correction into the combined function dipoles. Beta-functions are limited to 25 m, which corresponds to the maximum injected beam size around of 2 mm RMS in the vertical plane.

The lattice is composed of two families of combined-function dipoles BF and BD, together with three families of quadrupoles: QF, QD and QG (Figure 2). Three separate power supplies for the booster quadrupoles provide freedom in optimizing the lattice.

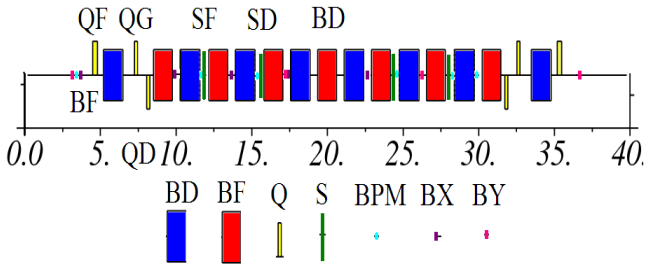

Figure 2: Sketch of the elements in one-quarter of the NSLS-II booster lattice. BF and BD are the focusing and defocusing dipoles, QF, QD and QG are the quadrupoles, SF and SD are the sextupoles, BX and BY are the horizontal and vertical orbit correctors, BPMs are the Beam Position Monitors.

Figure 3 shows envelopes of the beam injected from the linac. The phase space ellipse of the electron beam was matched to that of the circulating beam at the booster injection point. The RMS sizes of the injected beam envelopes are more than ten times smaller than the half-size of the vacuum chamber.

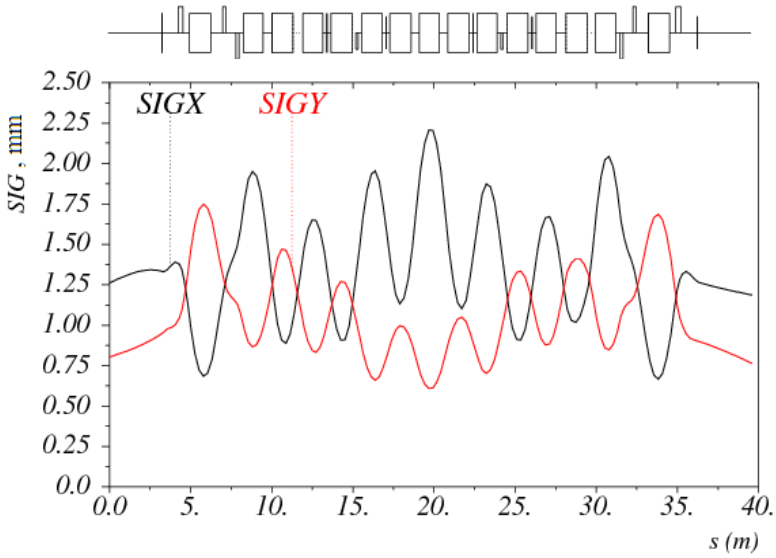

Figure 3: RMS injected beam envelopes in mm (solid curves) along a single booster quadrant.

In addition to the integrated sextupole component in the combined function magnets, four discrete sextupoles are introduced in every booster quadrant, shown as SF and SD in Figure 2. Separate power supplies for the sextupoles enable independent adjustments of horizontal and vertical chromaticity.

Table 2: Part Count/Magnetic Element Parameters.

Parameter	ASP Booster	NSLS-II Booster
Dipole parameters		
Number, BF/BD	28/32	28/32
Length, BF/BD	1.35/1.15 m	1.24/1.3 m
Angle, BF/BD	3.43/8.25°	3.27/8.39°
Injection energy	100 MeV	200 MeV
Field, BF/BD (inj)	0.015/0.042 T	0.031/0.075 T
Field, BF/BD (ext)	0.443/1.25 T	0.460/1.127 T
Quadrupole K1, BF/BD (ext)	0.82595/-0.66977 m^{-2}	0.82/-0.555 m^{-2}
Sextupole K2, BF/BD (ext)	3.54/-4.925 m^{-3}	3.5/-4.1 m^{-3}
Quadrupole parameters		
Number, QF/QD/QG	8/8	8/8/8
Length, QF/QD/QG	0.25/0.15 m	0.3/0.2/0.2 m
Quadrupole K1, QF/QD/QG	-2.351/0.4 m^{-2}	1.95/-1.36/1.433 m^{-2}
Sextupole parameters		
Number, SF/SD	8/8	8/8
Length, SF/SD	0.2/0.2 m	0.15/0.15 m
Maximum K2, SF/SD (ext)	50/-30 m^{-3}	30/-30 m^{-3}

Table 2 compares the main parameters of the proposed NSLS-II booster with that of the ASP booster [1]. The parameters of NSLS-II and ASP combined function magnets are chosen similar as shown in Figure 4. Increasing the injection energy from 100 to 200 MeV significantly increased the magnet fields at injection, which simplifies achieving required field quality of the combine-function dipoles.

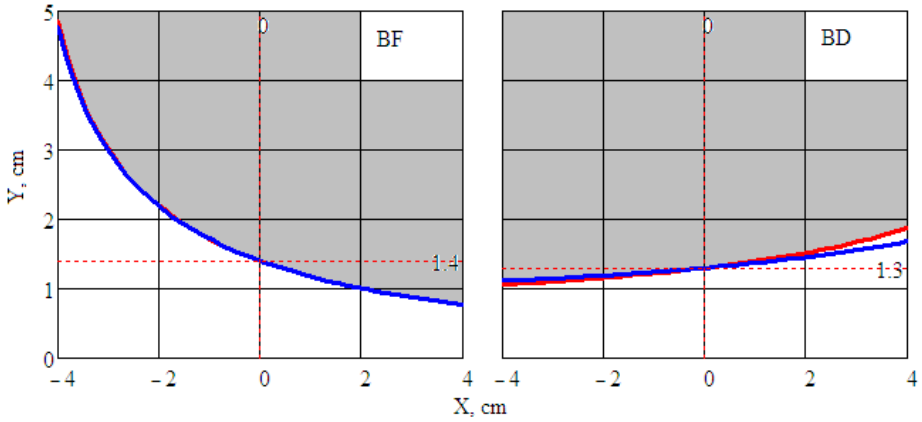

Figure 4: Magnet pole tip profiles[1], red – ASP, blue – NSLS-II.
Left plot corresponds to the focusing dipole; right plot corresponds to the defocusing dipole.

The main parameters of the chosen booster lattice are summarized in Table 3. The developed lattice is close to the ASP one; however with some modifications assuring that all of the requirements listed in previous section are fulfilled.

[1] Thanks to S. Mikhailov (Duke University) for his magnet design program.

Table 3: Booster Parameters.

Parameter	ASP Booster	NSLS-II Booster
Emittance, nm	34.4	39
Circumference, m	130.2	158.4
Booster current, mA	5	20
Revolution time, ns	434	528
RF frequency, MHz	499.654	499.68
RF voltage, MV	1.2	1.2
Harmonic number	217	264
X/Y tune	9.2/3.25	9.64/3.41
X/Y chromaticity	-8.83/-11.5	-9.9/-12.9
Expected X/Y coupling	5%	10%
Corrected chromaticities	+0.83/+0.87	+0.5 /+2
Momentum Compaction	0.0098	0.0084
Energy loss per turn, keV	743	686
X/Y/E damping time, ms	2.7/3.5/2.0	4.8/4.7/2.3
Damped energy spread, %	0.094	0.0082
Damped bunch length, mm	19	16.2

2. Lattice optimization

We explored the booster lattice performance in the tune space by tuning the QF and QD quadrupole families to adjust betatron tunes over the integer tune box around the working point in the bare lattice. This is important for the tune adjustment at injection and tune correction during energy ramp. Figure 5 shows the results of the tune scans. The plots show the maximum horizontal and vertical beta functions, the horizontal and vertical chromaticities, the horizontal emittance and the dynamic aperture. The working point is ν_x=9.64, ν_y=3.41.

The lower right quadrant of the tune space contains the most dynamic aperture. The maximum horizontal beta function stays around 12 m, with the maximum vertical beta function stays around 22 m over this quadrant. The horizontal chromaticity stays near 0.5 units. The vertical chromaticity drops from 2 units to 1 unit as the vertical tune is lowered from 3.5 to 3.0.

The booster emittance stays below 50 nm in this quadrant. The dynamic aperture at the working point is 1000 mm^2 which is larger than the physical area of 753 mm^2. The dynamic aperture is larger or comparable to the physical aperture over most of the lower right quadrant of the tune space. The large tuning range of the booster optics is beneficial for tuning the lattice for the best injection efficiency.

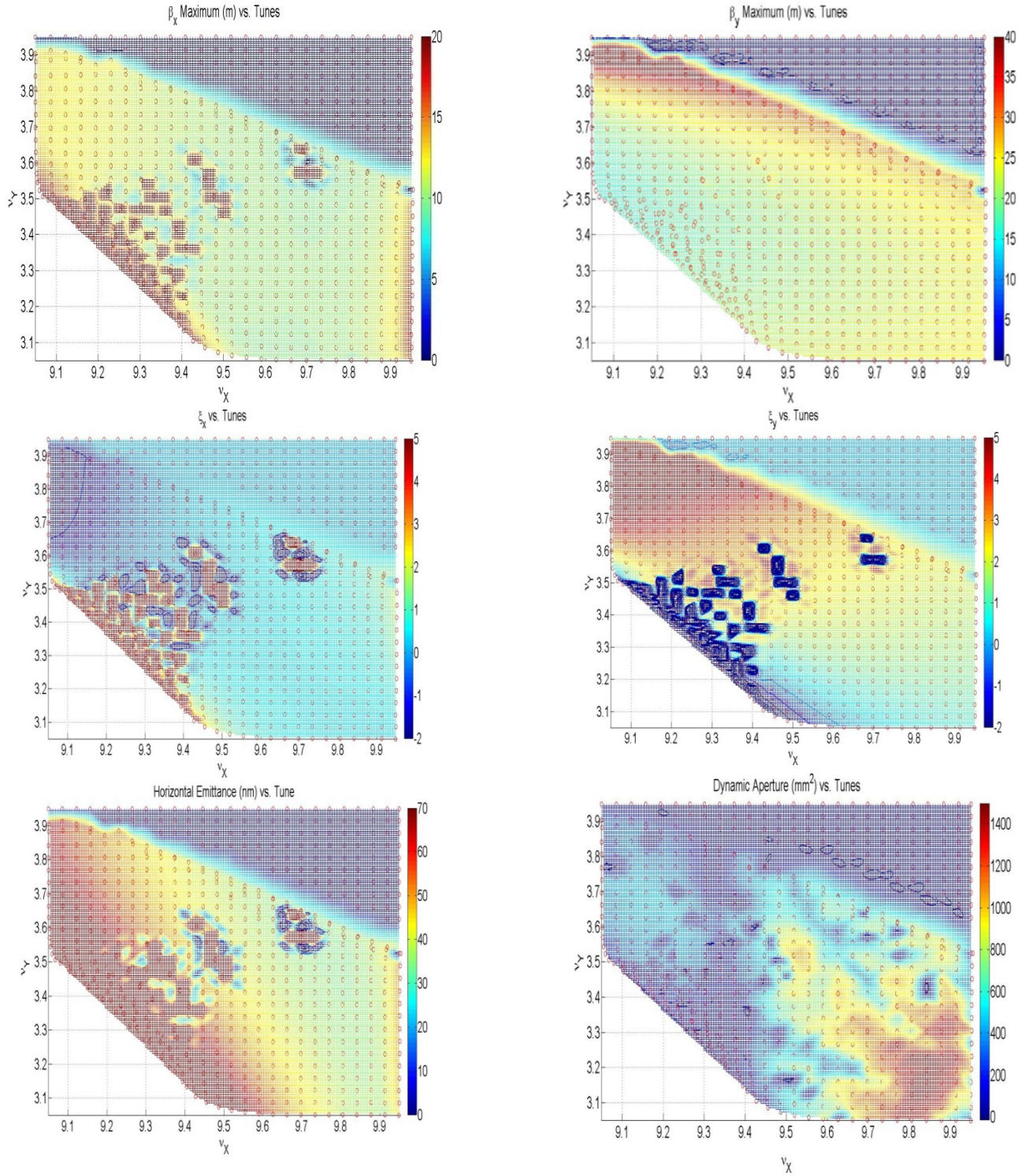

Figure 5: Tune scans of the lattice betatron functions [m], chromaticities, emittance [nm rad] and dynamic aperture [mm^2] for the bare lattice.

3. Lattice errors, their correction and impact on dynamic aperture

Preliminary consideration has been given to evaluation of the magnet tolerances and the orbit correction system. Table 4 shows the tolerances for the magnet alignment and fields that were assumed. Tolerances on the magnet parameters were developed using analytical estimates that assumed normally distributed random errors in all magnets. These tolerances are rms values, all simulations are done with a Gaussian distribution cut at 2σ.

Table 4: Magnet Tolerances.

Source of error	Tolerance
Dipole angle	0.02%
Dipole gradient	0.5%
Dipole transverse misalignment	0.150 mm
Quadrupole transverse misalignment	0.150 mm
Quadrupole gradient (relative)	0.5%
Quadrupole roll	0.200 mrad
Sextupole transverse misalignment	0.150 mm
Sextupole roll	0.200 mrad
BPM misalignment	0.150 mm
BPM roll	0.200 mrad

Orbit correction is implemented using 24 beam position monitors, 20 horizontal, and 16 vertical trim magnets. If necessary the trim fields will follow the energy ramp, enabling orbit correction at all energies. The developed trim–BPM arrangement allows correcting the booster orbit down to a 2 mm maximum deviation in each plane (Figure 6). This requires 1.5 mrad (maximum value) in the corrector strength, making its design simple, with low magnet weight and size. This orbit correction system results in alignment tolerances for the dipoles and quadrupoles summarized in Table 4. These tolerances can be relaxed further by further optimizing the corrector arrangement and adding one more vertical corrector magnet per quadrant.

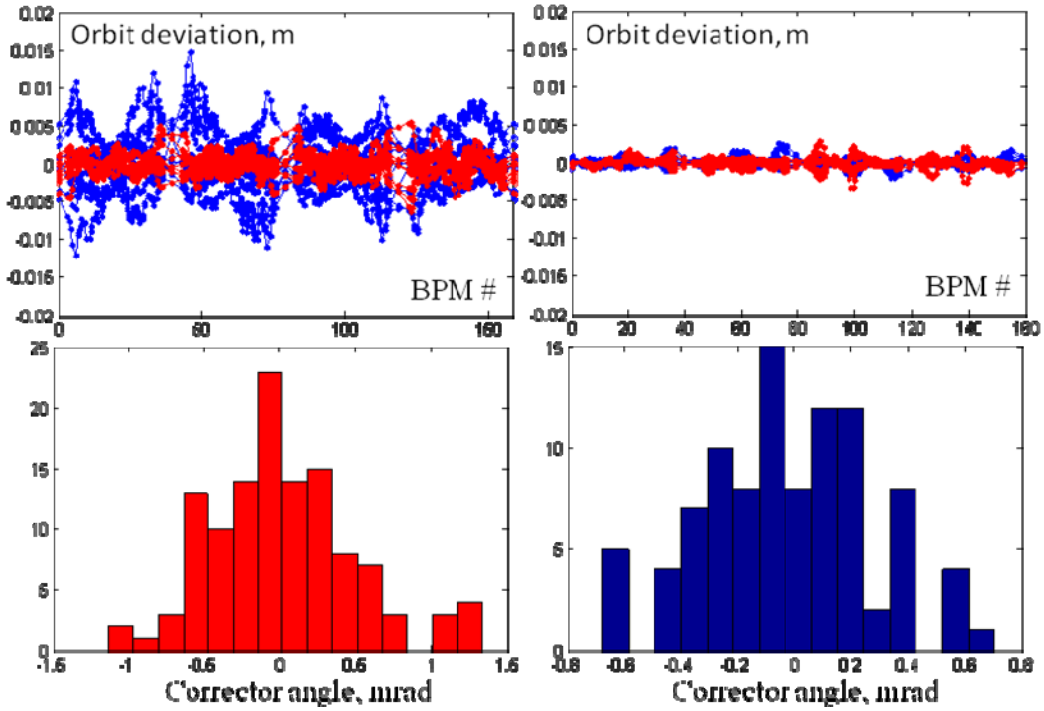

Figure 6: Uncorrected (left upper plot) and corrected (right upper plot) booster orbits. The two lower plots show the statistics of the corrector angles for 6 seeds of errors. Red and blue colors correspond to horizontal and vertical planes.

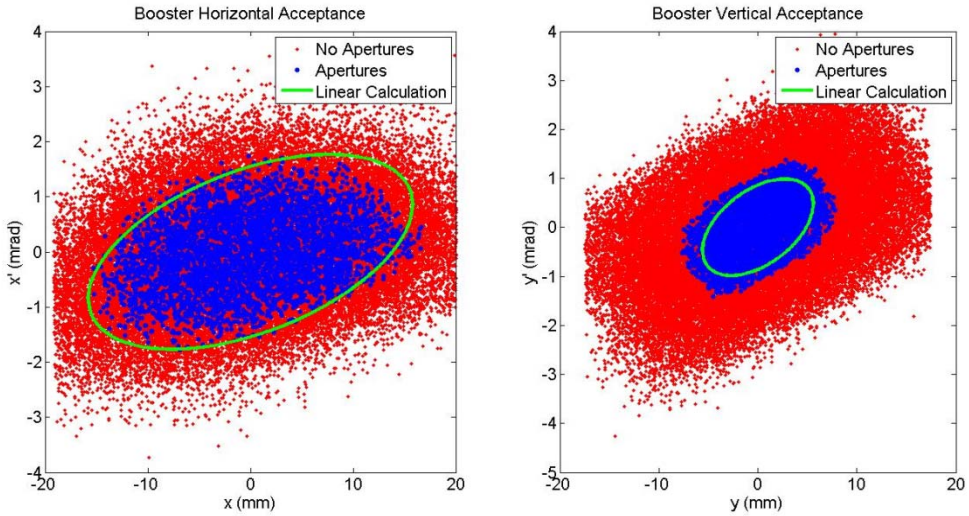

Figure 7: Booster Horizontal and Vertical Acceptance for the CD-2 version of the lattice. The green ellipse shows the acceptances calculated from the beam pipe aperture and twiss functions. The blue dots show an ELEGANT simulation of the booster lattice with errors at injection including apertures. The red dots are the same simulation without apertures.

The booster acceptance is an important parameter for injection efficiency. The anticipated apertures in the booster are 20 mm x12 mm elliptical half apertures. The booster acceptance determined in three ways. The first is a calculation using the twiss parameters to determine the ellipse that strikes the beam pipe. The second was an ELEGANT simulation of the bare lattice at injection including the apertures. The last was the same simulation without the apertures included. In both simulations the input phase space was painted to fill the physical aperture. The momentum spread was 5%. Figure 7 shows the results for the CD-2 lattice.

The simulation results with the apertures agree well with the calculated ellipses. The simulations without apertures show that the physical apertures limit the acceptance of the booster and not the dynamic aperture. Since the agreement between ELEGANT and calculation was quite good, the simulations were not performed for the current lattice, only the twiss calculations were performed. Table 5 shows the results the calculation for the final booster lattice design.

Table 5: Booster Acceptance

Phase space Variable	Limit	Acceptance
x	15 mm	30 mm-mrad
x’	2 mrad	
y	4 mm	3.6 mm-mrad
y’	0.9 mrad	
δ	5.5%	

Figures 8 and 9 show the horizontal and vertical booster acceptance limitation through one period of the booster. The horizontal aperture limitation is the QF magnet at the ends of the straight sections. The momentum aperture is the BF magnet in the center of the arc. The vertical aperture limitation is BD magnets at the ends of the arc sections. Figures 8 and 9 also show the 3σ beam size at extraction. The beam size at injection is approximately a factor of 3 larger. The beam size is much smaller than the acceptance.

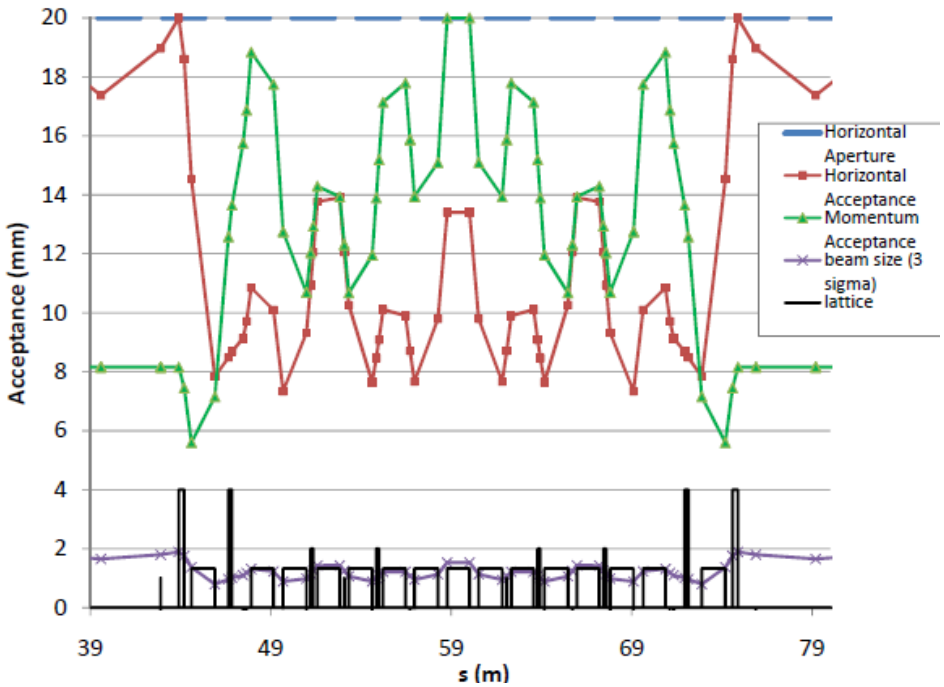

Figure 8: Horizontal aperture limitation along one quarter of the booster. The horizontal betatron acceptance and the momentum acceptance are shown as well as 3 σ beam size.

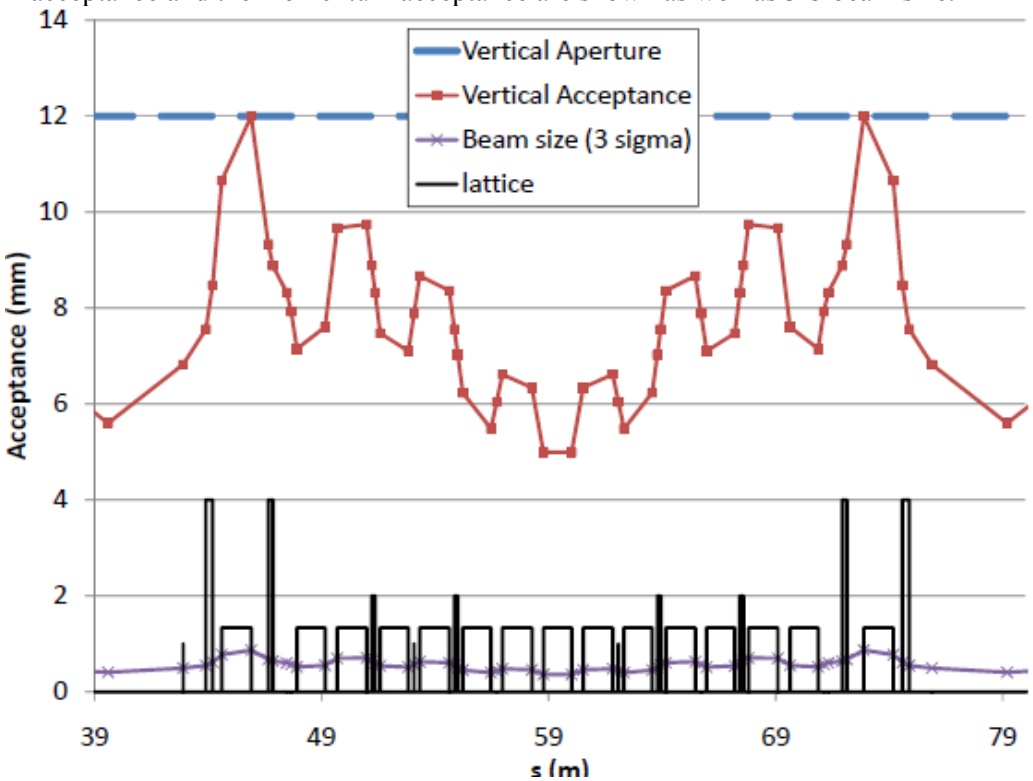

Figure 9: Vertical aperture limitation along one quarter of the booster. The vertical betatron acceptance and 3 σ beam size are shown.

The large tunability of the booster lattice should be maintained with the addition of realistic errors. Tune scans with errors were performed with the errors shown in Table 4. Two cases were considered. The first had not corrected the orbit, and the second included orbit corrections. Figure 10 shows the

dynamic aperture vs. the tune for the bare lattice, the lattice with uncorrected orbit and the lattice with the corrected orbit.

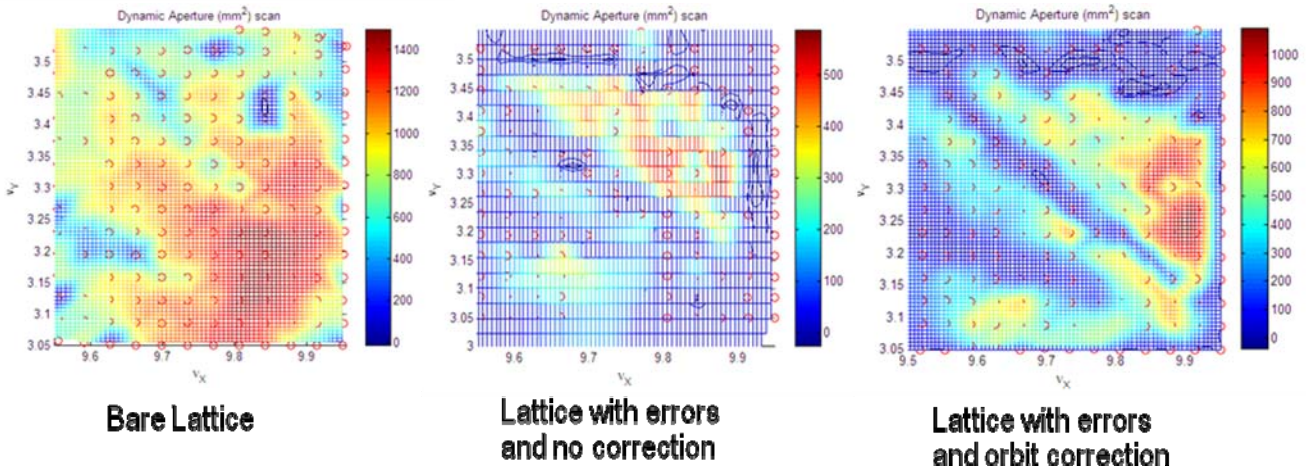

Figure 10: Dynamic aperture vs. tune for the booster lattice. The left plot is the bare lattice and is identical to the lower right corner of dynamic aperture plot in Figure 4. The middle plot shows the same tune space with errors included in the calculation. The right plot shows the effect of correcting the orbit on dynamic aperture.

These plots show that sufficient dynamic aperture at the working point and sufficient tunability of the lattice with these errors. Even though the orbit is not corrected, there is sufficient dynamic aperture in the booster, though it is not as large as the physical aperture. Correcting the orbit on the same lattice restores much of the original tune space and dynamic aperture. In fact, one can see from these plots that more dynamic aperture is available if the vertical tune is lowered and the horizontal tune is raised. Figure 11 shows the dynamic aperture at the working point with errors and orbit correction. The dynamic aperture fills the physical aperture and is larger than the stay clear aperture defined by the acceptance.

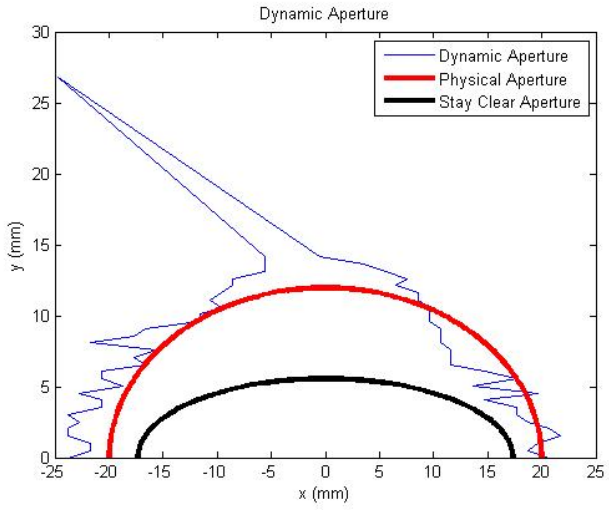

Figure 11: The dynamic aperture in the booster with errors and orbit correction. The dynamic aperture fills the physical aperture and covers the booster stay clear aperture.

Chromiticity is often a useful knob for coping with instabilities. The effect of vertical chromaticity on dynamic aperture was investigated at injection. Figure 12 shows the booster dynamic aperture for 2 values of the chromaticity at injection. The dynamic aperture reduced in the vertical when the chromaticity is increased from zero to two units. However, it is still larger than the physical aperture.

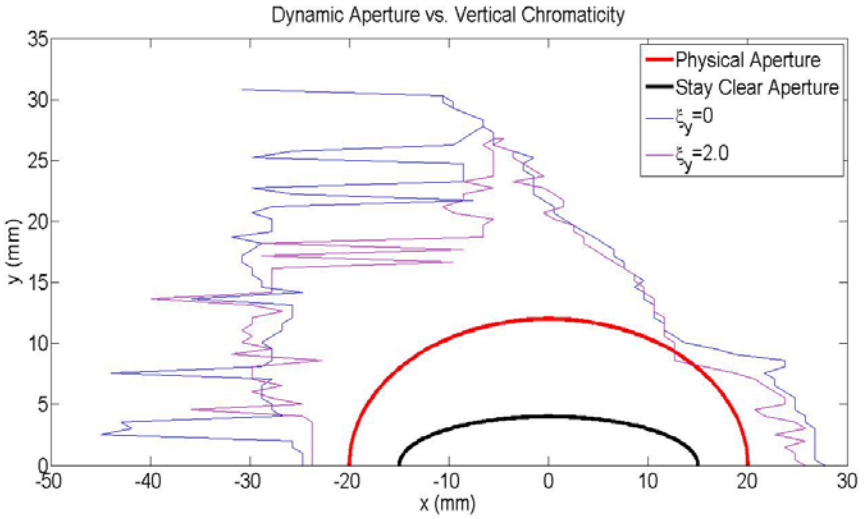

Figure 12: shows the change in tunes vs. amplitudes for the bare lattice.

Figure 13 shows the tunes vs. amplitudes in the booster. The vertical amplitude extends to the vertical stay clear. The horizontal stay clear amplitude extends to 25 mm-mrad out of a possible 30 mm-mrad. The tunes show acceptable variations vs. amplitude.

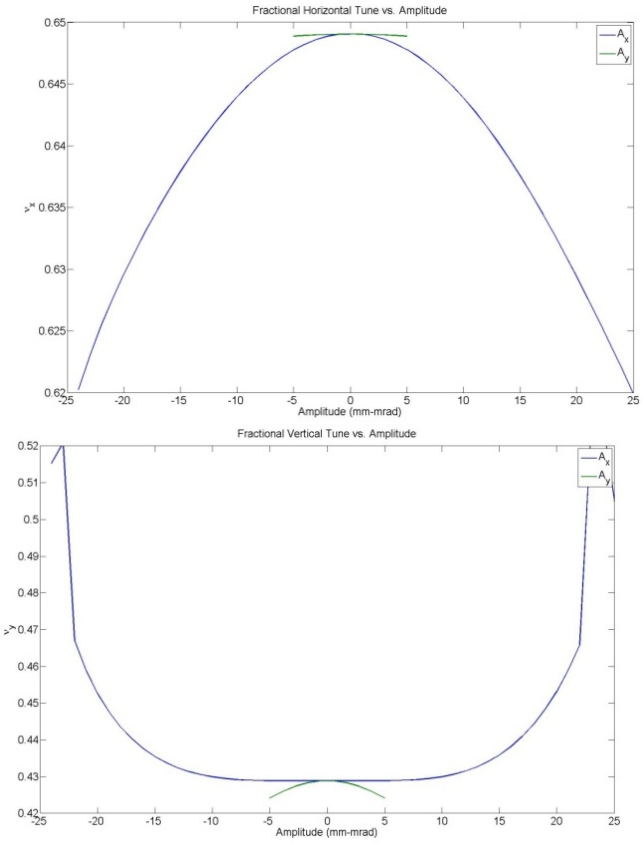

Figure 13: The left plot is the horizontal tune vs. horizontal and vertical betatron amplitude. The right plot shows the vertical tune vs. horizontal and vertical betatron amplitude.

Figure 14 shows the tune footprint for the booster beam. The horizontal position is varied ±16 mm, the vertical by ±5mm and the energy spread by ±0.012%. The particles are tracked for 2048 turns. Most of the tunes stay centered around the working point. Points far away are evidence of islands at large amplitudes.

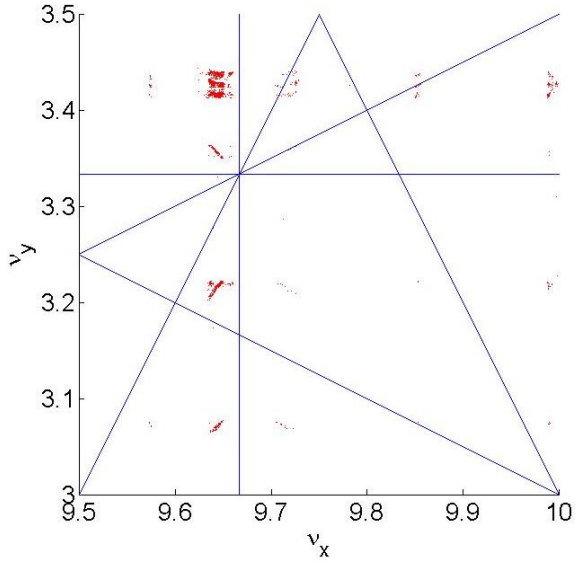

Figure 14: Tune space occupied by the beam in a lattice with errors and orbit correction. The blue lines show resonances up to third order.

4. Booster ramps

The short damping time at the maximum booster energy leads to a fully damped beam at the end of the ramp (Fig. 15). Here we assumed a sinusoidal ramp profile with the injection point "on the fly", i.e. on the rising slope of the energy ramp.

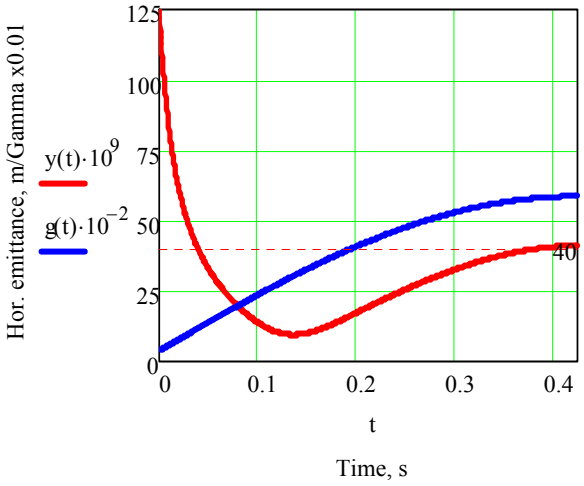

Figure 15: Booster energy ramp (in units of γ/100, blue curve) and dependence of the horizontal booster emittance versus ramp time (in nm·rad, red curve). Dashed line shows damped value of the booster emittance at 3 GeV.

Figure 16 shows the estimated beam loss throughout the energy ramp due to residual gas (mainly elastic scattering on the gas nuclei). Total relative charge loss is expected to be about 0.2% at the average value of the booster vacuum of 10^{-7} torr.

Figure 16: Relative gas-scattering losses in % of the charge (red curve) throughout energy ramp (blue curve).

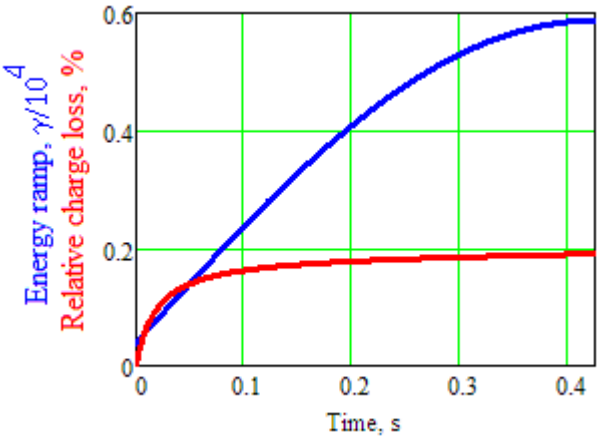

For an estimate of the chromaticity driven by eddy currents (Figure 17), we used a formalism developed in [8]. For the given lattice parameters, the estimated maximum value of the sextupolar moment is 0.085 m^{-3} at 1 Hz of repetition rate. Corresponding calculated values of chromaticity are about +0.5 horizontally and –1.4 vertically, which is much smaller than the natural chromaticity and can be compensated by ramping up SF and SD sextupoles.

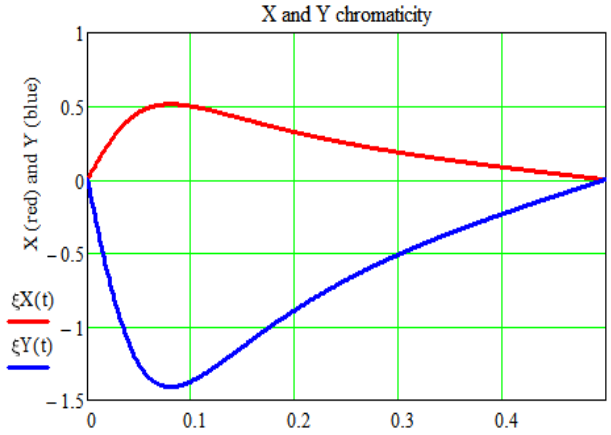

Figure 17: Eddy-currents induced chromaticity during the energy ramp. Red and blue curves show horizontal and vertical chromaticity correspondingly,

5 Booster Injection System

The booster injection system consists of the pulsed septum and four kicker bumps with their power supplies (Figure 18). It is a simple single turn on-orbit injection, allowing a maximum of about 150 consecutive bunches to be injected into the booster RF buckets. The bend angle of the septum is 125 mrad and that of the kicker is 12 mrad. This solution is viable and gives very reasonable field values for the pulsed magnets.

The injection system has the ability to transversely stack bunches from two linac pulses. The first linac pulse is injected on orbit with bumps BR3 and BR4, as in the normal case. When the second bunch train arrives, bumps BR1 and BR2 kick the first train 15 mm toward the septum knife. The septum knife is 20mm from the central booster orbit. The first and second trains will then be separated by 13mm at the exit of the septum. Bumps BR3 and BR4 will them kick the center of the pair of trains to the central orbit of the booster, so that each bunch will be 6.5mm from the central orbit. The bunches will merge together during the ramp.

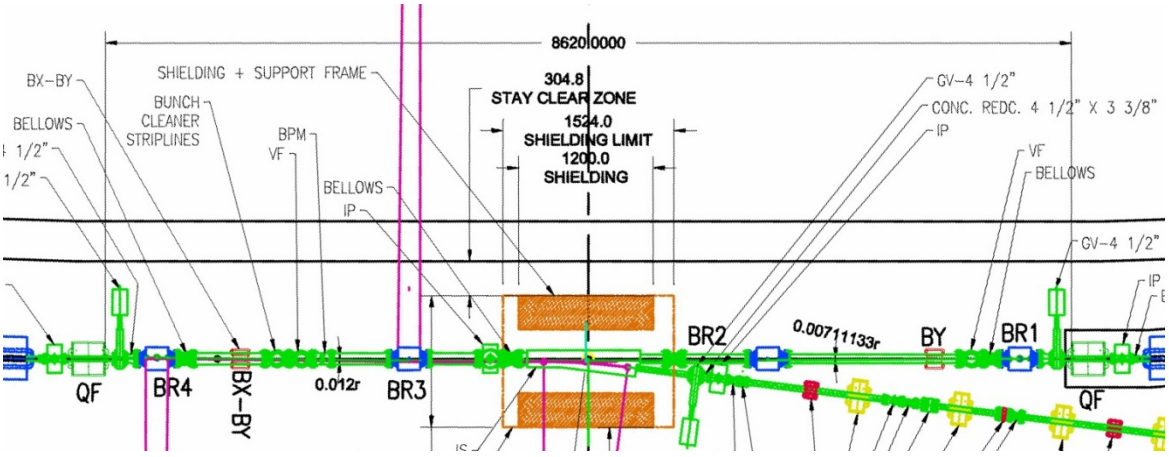

Figure 18: Booster injection system layout.

The basic magnet parameters are shown in Table 8.

Table 8: Booster Injection System Pulsed Magnet Parameters

Injection Energy 200 MeV	Booster Injection Septum	Booster Injection Bumps

Magnetic Field (T)	0.111	0.05
Length (m)	0.75	0.2
Magnet full gap H x V (mm x mm)	42 x 33	70 x 44
Bend angle (mR)	125	15
Inductance (μH)	1.2	0.4
Peak Current (A)	3210	1926
Drive Capacitor (μF)	211.2	PFN
Voltage (kV)	0.242	*
Pulse Shape	100 μsecfull sine	100 nsec risetime/fall time, 300 nsec flat-top
aMagnetic Material	¼ mm Si steel	CMD5005
Ceramic Chamber Coat	N/A	2 – 3 Ω/ Ti

*The drive voltage depends on the PFN configuration and matching system

The capacitor banks or transmission line PFN's are charged with voltage regulated DC power supplies with up to 16-bit resolution voltage regulation. The transmission line for the injection kicker is terminated with a de-Q'ing circuit to pull the current/field down before the head of the injected bunch train re-enters the kicker after completing one revolution in the booster. The system impedances need to be matched carefully to prevent excessive ringing, although the requirements for the booster injection system are not nearly as stringent as for the booster extraction. Emittance dilution with consequent lossy injection into the storage ring are rapidly produced as the extraction magnet specifications are exceeded (see below). For booster injection, current (field) stability, pulse-to-pulse reproducibility and ripple/droop may be of the order of 1%.

6 Booster Extraction System

The booster extraction system consists of four slow orbit bumpers, pulsed and DC septa and kicker (Fig. 19). The orbit of the circulating bunch train is moved out toward the extraction septum over several hundred turns by the slow orbit bumps and is kicked into the extraction septum by the extraction kicker [12]. The arrangement is shown in the plan view below, and the magnet specifications are outlined in Table 9.

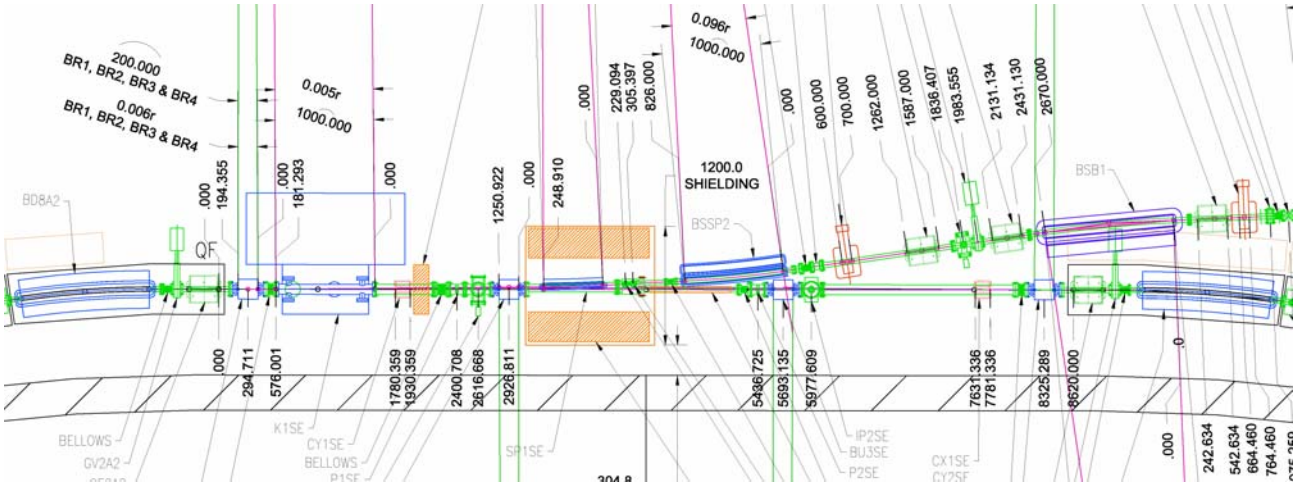

Figure 19: Booster Extraction Section

The extraction septum is split into two magnets – short and weak pulsed and relatively long and strong DC magnets[2]. Constraints on the magnet parameters and their arrangement were the following:

- clearing the extracted beam trajectory off the downstream quadrupole
- having sufficient value of the closed bump amplitude at the location of the extraction septum
- minimizing the pulsed septum and maximizing the DC septum strengths
-

Table 9: Pulsed magnet parameters for the extraction system (Fig. 20)

Pulsed Magnet	Length, m	Angle mrad	Field, gauss	Peak Current, A	Peak Voltage	Pulse width, μs	Relative error, %
Bumper	0.2	7.5	3750	722/20 turns	363	1000	0.02
Kicker	1	5	500	1926	*	0.2/0.3	0.2
Pulsed septum	0.6	48	8000	16110	1062	100 full sine	0.02

*Voltage depends on PFN configuration and matching.

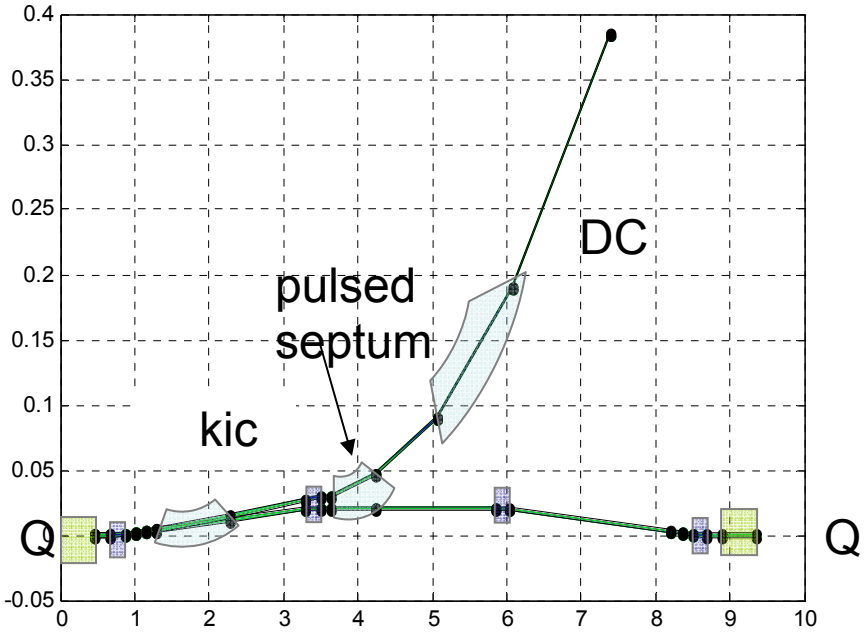

Figure 20: Booster extraction system layout. Lower curve is the stored beam trajectory when the extraction bump is on. Higher curve is the extracted beam trajectory. Horizontal and vertical scales are in meters. Thickness of the line corresponds to the local 6 RMS beam envelope.

The tolerances on the stability, reproducibility and ripple/droop of the extraction kicker are very stringent. These parameters govern the effective emittance of the extracted beam, and must not be exceeded. Reproducibility of the pulsed septum waveform of about 0.02% is

[2] Suggested by S.P. Möller.

difficult and requires feed-forward but is feasible. The ripple and droop of 0.2 % over the entire kicker flat-top of 300 nsec waveform, especially with a rise-time of <200 nsec is very difficult to obtain and will require special techniques.

Figure 21 motivates the reason for the tight tolerances on the ripple/droop of the extraction kicker. The red ellipse is a bunch that is not affected by the ripple/droop of the extraction kicker. The blue ellipse is a later bunch in the same train that is kicked 0.2% more at the kicker. The black ellipse is the ellipse encompasses both bunches and corresponds to the ellipse that will be measured. The measured emittance will increase 20% in this case.

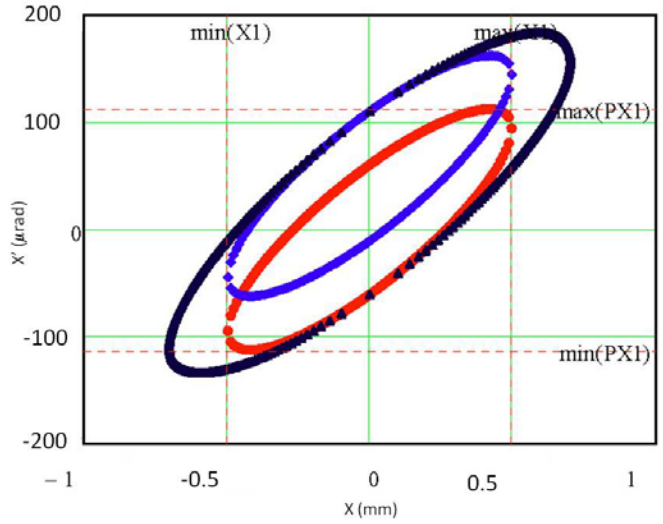

Figure 21: Apparent emittance blowup from ripple. Red and blue ellipses represent 2 bunches in a bunch train. The blue is deflected differently from the red due to ripple in the extraction kicker. The black ellipse is the apparent ellipse of the two bunches together.

7 DC Extraction Septum

The extraction system of the NSLS-II booster contains two septa magnets. Total angular kick of 140 mrad is split between two magnets, pulsed and DC, in order to reduce the requirements on the pulsed magnet power supply, whose stability is much more difficult to achieve and maintain as compared with the DC power supply. The optimum distribution of the trajectory bending angle between these two magnets is 46 mrad for the pulsed magnet and 96 mrad for the DC one. The main problem with the DC magnet design must accommodate the booster vacuum chamber. The magnet design, which needs to be compact enough to fit in the small space constrained by the vacuum pipe, must not exhibit significant stray fields since these fields will disturb the orbit of the electron beam circulating in the booster. The integral stray field in the booster vacuum chamber shall be less than 1 Gauss-meter, while the magnet will operate at a high field corresponding to the extraction energy of 3 GeV, however, the circulating booster beam may have the energy as low as 200 MeV (the energy value at the booster injection).

As a result of these considerations the following requirements were developed on the magnet and its power supply. The booster extraction septum parameters are described in the table below.

Table 10: Booster Extraction Septum Parameters

Magnetic length	1 m

Magnetic field (nominal)	0.96 T
Full gap	2 cm
Pole width	5 cm
Good Field Region (GFR)	H1cm x V4cm
Field tolerance within GFR	0.1%
Current (nominal)	215A
Voltage (nominal)	7 V
Current ripple	0.01%

As for the magnet geometry the following layout was developed and tested with a 2D magnetic simulation code.

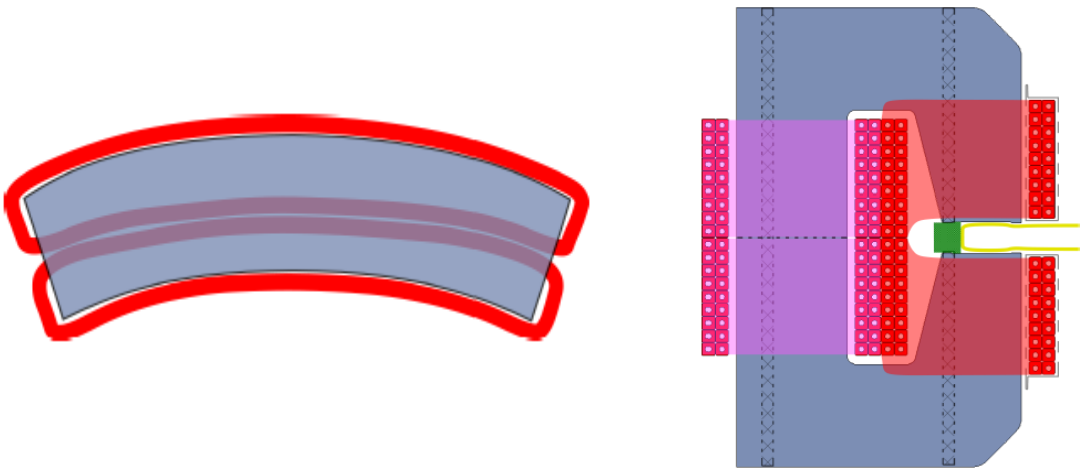

Figure 22: Top-view and cross-section of the magnet with four sets of coils.

This design will require splitting the magnet yoke for the coil assembly. However, the design offers a minimum field of below 1 Gs across the booster vacuum chamber. Also the field uniformity across the gap is below 0.02%, which exceeds the actual specification.

In order to protect the booster beam from the DC septum stray field, magnetic shielding is used, as shown below. The shield may be comprised of a cm-thick magnetic cylinder wrapped around the booster vacuum chamber in the vicinity of the DC extraction septum. One way of manufacturing the shield is splitting the cylinder in half along the longitudinal axis and installing both halves together using metallic tie wraps to hold both halves intact.

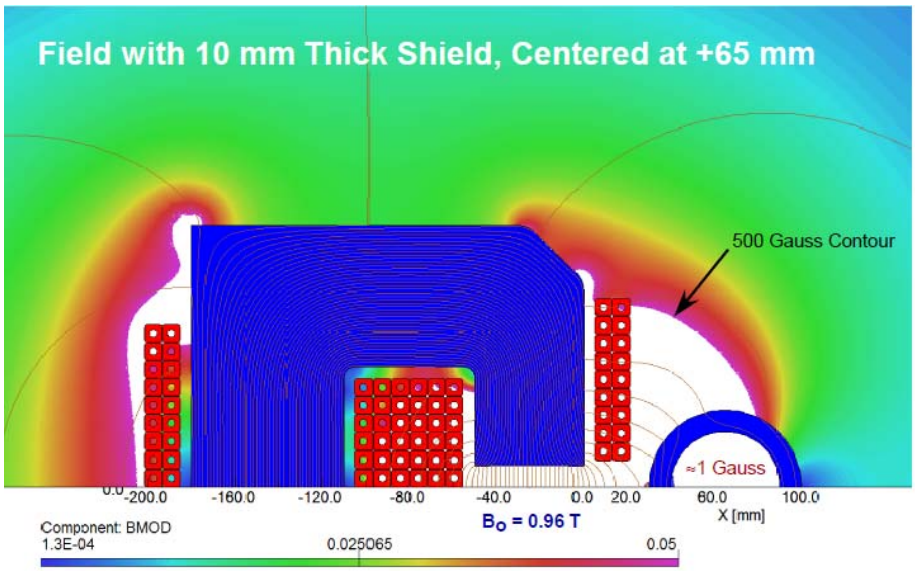

Figure 23: Field map of the magnet.

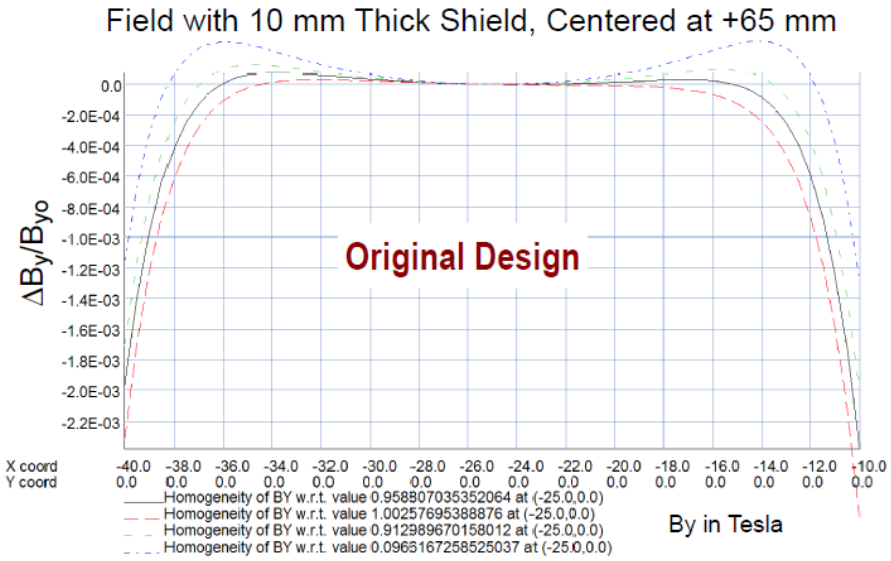

Figure 24: Vertical field dependence across the pole.

8 Beam Diagnostics

The beam diagnostics system will enable continuous monitoring of the following beam properties:

- Current
- Horizontal and Vertical Tunes
- Orbit
- Beam shape
- Fill pattern

Booster instrumentation is summarized in Table 11 below. Six fluorescent screens will be installed to facilitate booster commissioning and troubleshooting. Booster orbit will be monitored with 24 BPMs with turn-by-turn capability. The BPM receivers will be provided by BSA. Circulating current will be measured with DCCT, while fill pattern will be monitored with a fast current transformer. For tune measurement, the electron beam will be excited using striplines. The beam response will be observed with dedicated striplines. The spool with the length of stripline should be provided for future installation of bunch cleaner system. Synchrotron radiation from a dipole will be used to observe the beam during ramp and emittance measurements. An additional optical port to monitor bunch length with a streak-camera will also be provided. The supplied equipment and subsystem components should be capable to operate in the harsh accelerator environment (EMI, radiation, etc).

Table 11: Diagnostics/Instrumentation for booster

Qty	Spare	Monitor Type	Abbrev	Measured Beam Parameter
1	1	DC Current Transformer	DCCT	Beam Current
1	1	Fast Current Transformer	FCT	Fill Pattern
6	1	Fluorescent Screens	FLAGS	Intensity, Beam Shape & Position
2	1	Strip Line	SL	Tune Measurement System
24	2	Beam Position Monitor	BPM	Beam Position, Orbit

These systems will include:

- ***Beam Position Monitors –*** Will consist of four RF pick-up electrodes. The PUE feedthroughs with a characteristic impedance of 50 Ohms will be equipped with female SMA connectors. There are a total of 24 BPMs which will measure beam position and orbit. The power levels of 498.68 MHz at the input of the BPM receiver should not exceed -10 dBm with 30 mA in 80 bunches and should be at least -50 dBm with 1 mA of circulating current in 150 bunches. Peak voltage at the input of the receivers should not exceed 80 V.
- ***DC Current Transformer and its electronics*** **-** Will be used to measure beam current, lifetime and injection efficiency, and will be a device consisting of the following specifications~~:~~: Range 0-50mA; resolution of <5μA / $Hz^{½}$; bandwidth from DC to 10kHz; output voltage range from -10 V to +10 V . Reference Bergoz part #NPCT-115-C100-H, in-flange version is requested. A TTL compatible timing trigger signal is also required. The receiver electronics will consist of 16 bit ADC with sample rate at least 1 kHz, and will comply with integration specifications for control system.
- ***Fast Current Transformer and its electronics –*** Will be used to measure individual bunch charges (intensity), fill pattern. Reference Bergoz part # FCT-WB-082-20:1 is a passive transformer consisting of the following specifications: sensitivity of 1.25V/A; 1.75 GHz bandwidth; 200 ps rise time, characteristic impedance of 50 Ohms; bipolar output signal. The

receiver electronics will consist of PCI express multi-channel fast ADC (Ref. Acqiris DC271A), and will comply with integration specifications for control system.

- ***Fluorescent Screens (beam flags) and their optics and cameras*** - Will be used to measure transverse profile and beam position and may consist of an integrated system of components that can be reconfigured and interchanged, whereby Cerium doped Yttrium Aluminum Garnet (YAG:Ce) screens can be swapped out of a UHV (Ultra High Vacuum) compatible body with ease. The flag design should provide capability of calibration of imaging system. The resolution should be better than 50 μm covering a field of view of approximately 20 mm. Beam image will be captured using CCD camera consisting of or equivalent to the following specifications: resolution of 1.3 Megapixel or better; dynamic range of 1,800:1; 12bit ADC; external trigger capability; external control and interface via Gigabit Ethernet. Reference RadiaBeam Technologies part # IBS-xx and Hamamatsu Digital CCD Camera part # C8484-05 Series. Qimaging Digital CCD Camera part # QIC-F-CLR-12-C, Flea miniature IEEE-1394b Camera (Point Grey Research).
- ***Synchrotron Radiation Monitor*** - Will be used to measure beam profile and beam size of the synchrotron radiation light source for performance optimization, routine operation check, and various beam physics study. The monitor should have the ability to resolve small transverse beam dimension and motion, with resolution of better than 50um in each plane. The Synchrotron Radiation Monitor will consist of image forming optics, image capture CCD digital camera and analysis tools. Beam image will be captured using CCD camera consisting of or equivalent to the following specifications: resolution of 1.3 Megapixel or better; dynamic range of 1,800:1; 12bit ADC; external trigger capability; external control and interface via Gigabit Ethernet. Provisions for extra port (Bending Magnet Port) to be used to implement streak camera. Reference Hamamatsu Digital CCD Camera part # C8484-05 Series. Qimaging Digital CCD Camera part # QIC-F-CLR-12-C, Flea miniature IEEE-1394b Camera (Point Grey Research).
- ***Tune Measurement System*** - Tune measurement system shall enable measurement of the booster tunes in the range of ± 0.5 around the designed working point with the resolution of better than 0.05. The system will utilize two identical stripline assemblies. One assembly will be used for the beam excitation, while another shall provide beam response signal. The striplines shall be capable to withstand 300 W RF power. The system shall reliably provide tunes data for a single bunch charge of 100 pC and for a train 150 bunches with 10 pC/bunch. The tunes data shall be available to the injector control system during whole energy ramp duration between beam injection and extraction in at least 20 time steps. The system shall have an ability of magnifying the tune range of interest and provision of sampling every booster ramp.

9 Beam Chambers and Vacuum System

The booster ring vacuum system includes all vacuum chambers, vacuum pumps, vacuum instrumentation and diagnostics, vacuum controllers, and connecting wiring.

An average pressure below $1x10^{-7}$ Torr is needed within the booster to minimize the beam loss and bremsstrahlung radiation due to beam-residual gas scattering. The booster vacuum system will be designed with sufficient pumping capability to achieve vacuum pressures in the 10^{-8} Torr range. Most booster vacuum chambers will be constructed from seamless stainless steel tubing and will utilize Conflat flanges.

The booster vacuum will be divided into eight sections isolatable with all metal or radiation-resistant EPDM-sealed gate valves. The four arc sectors will be ~ 31 m each and the four straight sections of about 8 m each. Each arc sections will have 15 bending chambers of ~ 1.5 m long for BF and BD magnets, and short straight pipes for multipole magnets, bellows and side ports for appendage components such as pickup electrodes, gauges, roughing valves, ion pumps, etc. The four straight sections will house injection, extraction, RF cavities and beam diagnostics. Conventional ultra-high vacuum technology will be implemented. High vacuum will be achieved with small sputter ion pumps distributed around the booster ring.

The booster will accelerate the 200 MeV bunch train from the linac to the full energy of 3 GeV at 1 Hz repetition rate. To minimize the eddy currents during the fast ramping fields (and the associated sextupole effect), the vacuum chambers will be made of thin-wall stainless steel. A wall thickness of about 0.7 mm is sufficiently strong for a bending chamber with an elliptical inner cross section of 25 mm (V) × 40 mm (H), while having sufficiently low eddy currents. The 60 bending chambers will be about 1.5 m long with bending radii of 10 m and 23m for defocusing and focusing chambers, respectively. They will be made from seamless stainless tubing, drawn and pressed into elliptical shape, then roll-curved to give the required bend angles. The ends of the bending chambers may be tapered from elliptical to round cross-section and welded to Conflat flanges. The maximum stress and deflection of the bending chamber under the external atmospheric pressure occurs at the top and bottom of the chambers. Using finite element analysis, the stress and deflection are found to be 11000 psi and 0.2 mm, respectively (Figure 25), which is well within acceptable ranges with large safety margins.

The straight drift pipes between bending chambers will have similar inner dimensions as the bending chambers and made of thin wall stainless steel. Each drift pipe consists of a section for multipole magnets, mounting for four BPM buttons, a cross for vacuum pumps and gauges, and a short bellows. Conflat flanges will be used throughout the booster ring.

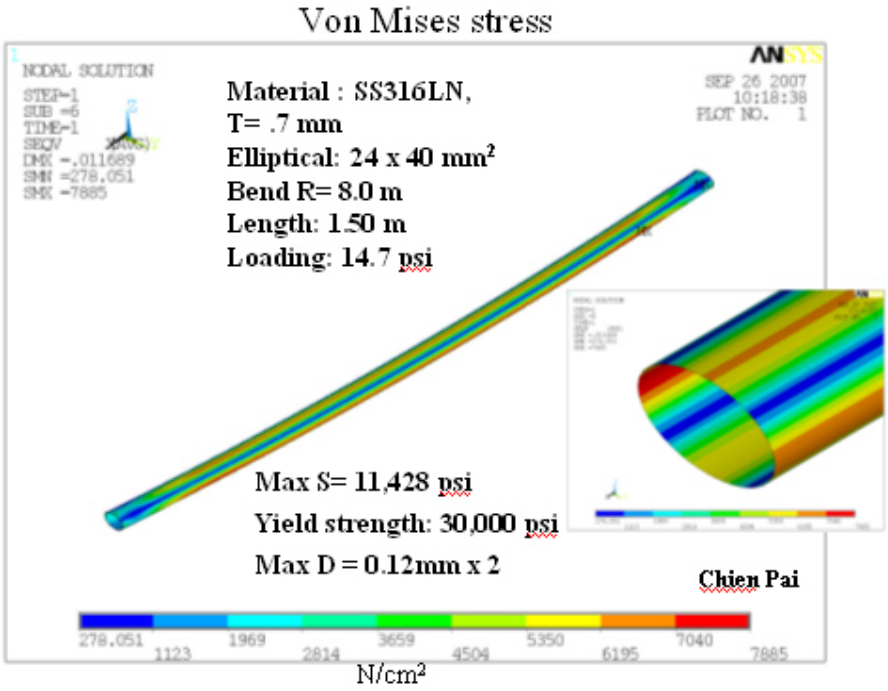

Figure 25: Calculated stress of the thin-wall bending chamber under vacuum load. The high stress is at the side of the tube along the horizontal plane with maximum stress of less than 11kpsi. The calculated deflection is ~0.2 mm.

After proper chemical cleaning, the completed chambers and drift pipes will be vacuum degassed at 450ºC in a vacuum furnace for several days to remove any trace of surface contaminants and to reduce outgassing, eliminating the need for in-situ baking. The chambers and the pipes are then assembled into the magnets and tested prior to installation in the tunnel. Once they are installed and connected to other beam pipes, two gate

valves will be mounted at the end of arc sections, so each section can be individually pumped down to high vacuum.

The thermal outgassing of the clean stainless chamber surface will be less than $1x10^{-10}$ Torr-l/s/cm^2, 24 hours after pumping down. This is equivalent to a total thermal gas load of ~$2x10^{-5}$ Torr-l/s for the whole booster ring, excluding the contributions from RF, injection, extraction, and diagnostics. The pressure in the booster will be dominated by the synchrotron radiation-induced desorption during operation at 1 Hz. This effect will be much less pronounced during the top-off injection mode due to low duty factor. Assuming a 20 mA multi-bunch beam accelerated to 3.0 GeV in the booster during the 0.4 sec acceleration cycle, the average synchrotron radiation power on the vacuum chamber wall will be less than 1600 W for the whole ring, concentrated at the downstream end of the dipole chambers, with a linear power density less than 40 W/m. No observable temperature rise at the chamber wall is expected.

The average photon flux during acceleration is approximately 1×10^{19} photons/sec. Assuming a PSD yield of $\eta = 2\times10^{-4}$ molecules/photon, the total photon-desorbed gas load will be about 1×10^{-4} Torr-l/s, which is much higher than the thermal desorption gas load. Desorption yield of $\eta = 2\times10^{-4}$ mol/ph can be achieved with an integrated dosage of 10^{19} ph/meter, reached in a few hours of continuous booster operation. Both the thermal- and photon-desorbed gas load will be handled with the 30 l/s ion pumps at the downstream end of each bending chamber. The pressure distribution in booster arc section can be estimated using standard linear conductance formulae and super imposing photon stimulated desorption over the thermal desorption. The pressure distributions of a 10 m long arc section for three different pumping schemes are plotted in Figure 26, with one 30 l/s ion pump downstream of each bending chambers (~ 2 m pump spacing); with one 100 l/s ion pumps downstream of each bending chamber; and with one 30 l/s ion pump at every other bending chambers (~ 4 m pump spacing). The average pressure for 1st case is about 1.2×10^{-7} Torr and 25% lower with 100 l/s ion pumps. Due to the limited conductivity of the small-diameter beam pipes, the average pressure will improve with shorter pump spacing, rather than with larger ion pumps, as illustrated in the 3rd case, where pressure increases by factor of 3 when number of pumps is halved. The average pressure will improve rapidly to mid 10^{-8} Torr within a week, since η decreases with integrated beam dose and thermal outgassing decreases with time.

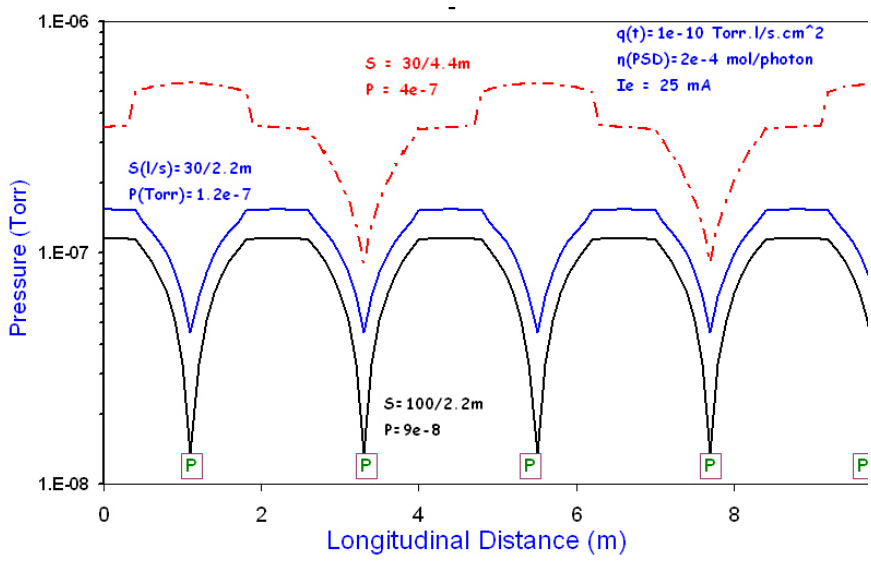

Figure 26: Pressure distribution in booster arc sections from both thermal desorption and photon-stimulated desorption. Each arc section will have fifteen 30 l/s ion pumps, at downstream end of each bending chamber (black curve). Due to the limited linear conductance of the small diameter beam pipes, the average pressure only decreases by 25% if 100 l/s ion pumps are used instead of the 30 l/s pumps (blue curve). The average pressure will increase three folds if only one ion pump is installed for every two bending chambers (red curve).

The booster ring vacuum sectors will be roughed down from atmospheric pressure with portable turbo-pumps (TMP) backed with dry mechanical pumps before transferring to the sputter ion pumps. Two right-angle, all-metal valves will be mounted at each vacuum sector for roughing, bleed-up, and for other vacuum diagnostics. The

TMP stations will have their own vacuum gauges and an electro-pneumatic valve to isolate the TMP from the vacuum section in the event of pump or power failures. The TMPs will be manually isolated with valves, once each booster ring sector is at high vacuum. Large ion pumps of about 200 l/s, identical to those deployed in the storage ring, will provide sufficient UHV pumping speed at the straight sections for RF cavities, injection, extraction, and diagnostics.

Power supplies and controllers for linac and booster vacuum systems will be located in the satellite electrical racks in the injector service area. Commercial dual ion pump controllers and vacuum gauge controllers with local and remote capabilities will power, monitor, and control the ion pumps and vacuum gauges, and interface with the PLC and control computers. Ion pump currents and the vacuum gauges will provide information on the pressure distribution in the booster ring.

The booster vacuum will be monitored and interlocked with the ion pump current and the vacuum gauge readings. Each arc vacuum section will have a convection-enhanced Pirani gauge (TCG), two inverted-magnetron cold cathode gauges as the primary gauges, and fifteen 30 l/s ion pumps. One set of vacuum gauges and two large ion pumps will be installed at the short straight sections to handle the extra outgassing from RF cavities, kickers, septa and diagnostics. Residual gas analyzer heads will also be installed at short straight sections for diagnostics during operation and maintenance periods. A residual gas analyzer head may be mounted on the portable TMP stations to assist the pumpdown and troubleshooting of arc vacuum sections. Table Vacuum 1 presents a list of booster vacuum devices, together with those for linac and beam transport lines.

Table 12: List of Vacuum Components for the Linac and Booster Vacuum Systems

	IP (30 l/s)	IP (200 l/s)	TCG	CCG	TMP	RGA	GV
E-gun	2	2	2	2	1	1	2
GtL		2	1	2	1		2
Linac		8	4	8	1	1	2
LtB	8		2	4	1		2
Booster	60	8	8	12	4	3	8
BtSR	18		2	4	1	1	2
Total	72	20	18	30	10	6	18

The vacuum control system will interface with vacuum devices while being part of the machine control. Due to the high radiation levels in the tunnel, all the vacuum devices will be located at the satellite control racks. These vacuum devices (such as gauge controllers, ion pump controllers, RGA, etc.), with local and remote capabilities, will communicate with the machine control system through RS232 or Ethernet links for remote monitoring, operation, and control. The low-level vacuum control will consist of dedicated vacuum programmable logic controllers. Each PLC has both digital and analog I/O modules with inputs from various vacuum devices, and provides the logic for the operation of the sector gate valves, the interlocks for other subsystem devices, and generation of the beam permits. For the gate valve control, a voting scheme with inputs from the setpoint contacts of several ion pumps will be used to initiate the interlock functions, therefore minimizing false triggering due to the failure of a single pump.

10 Booster Power Supplies and Electrical Utilities

Power Supplies

Power supplies will be designed to match the requirements of the booster magnet lattice and meet the ramp requirement for **1** Hz operation. Stability and current ripple specifications will also be derived from the machine requirements. It is expected that these power supplies will be high precision current controlled devices. The high current dipole and quad power supplies will have to operate in two quadrants to enable a fast down ramps to meet the 1 Hz cycle frequency. The sextupole and corrector magnets will use bipolar power supplies. There is one power supply for each sextupole and corrector magnet. The current setpoint will accomplished through an analog voltage going to the power supply regulator circuit. The larger dipole power supplies will use a energy leveling system to minimize the disturbance of the AC power lines by drawing significantly less than the peak AC current during a cycle.

The following table is a summary of operating parameters for the NSLS II booster using conceptual deigns for the different types.

Table 13: Preliminary Operating Parameters For NSLS II Booster Power Supplies

PS Type	Mag. Qty Per CKT.	# CKTs	Mag. Curr.	Mag. Resist.	Lead Resist.	Resistive Voltage	Magnet Induct.	Ramp Up Time Sec.	Inductive Voltage	Peak Voltage	Peak Output Pwr
BR- BF	28	1	907	0.0070	0.0108	187.6	0.0007	0.26	68.4	255.9	232139
BR- BD	32	1	732	0.0210	0.0108	499.8	0.0076	0.26	684.7	1184.5	867062
BR-QF	8	1	157	0.1020	0.0408	134.5	0.0150	0.26	72.5	207.0	32496
BR-QD	8	1	85	0.0450	0.0675	36.3	0.0050	0.26	13.1	49.4	4200
BR-QG	8	1	126	0.0450	0.0675	53.9	0.0050	0.26	19.4	73.2	9229
BR-SXV	1	8	18	0.3530	0.5525	16.3	0.0160	0.26	1.1	17.4	2507
BR-SXH	1	8	18	0.3530	0.5525	16.3	0.0160	0.26	1.1	17.4	2507
BR-Corr	1	32	7	0.3270	0.8670	8.4	0.0150	0.26	0.4	8.8	1963
										Total Peak Power	1152102

All power supplies will have sufficient interlocks to prevent the power supply from damage due to changes in cooling conditions, AC power disturbances, and out-of-range setpoints. All magnet coils will have an over-temperature interlocks to prevent damage due to a change in cooling or operating conditions. One of the dipole power supplies will have an electrical safety interlock that will prevent the power supply from turning on if the booster personal safety system requirements so warrant. All power supplies are to be remotely operated by the power supply control system. All power supply faults will be latched and require a remote reset to clear the faulted interlock. All power supplies will conform to the latest BNL safety requirements, especially concerning arc flash protection. Whenever possible, NRTL-listed equipment will be used.

Power Supply Controls

The power supply controls will be the same hardware that is being developed for the NSLS II storage ring. They will consist of a PSI (Power Supply Interface), PSC (Power supply Controller), Cell Controller, and IOC. The PSI is located at each power supply and is connected to the power supply controls. The PSI generates an analog current reference for a power supply and has a number of analog input channels for monitoring power supply signals. The resolution of the analog current reference is 18 bit and the analog input to the PSI are 16 bit. The PSI also has digital input/output lines to control the state of the power supply and read back the status. The PSI is connected to the PSC by fiber optic cables for electrical isolation. The PSC is where the ramps are generated and monitoring signals from the PSI are loaded into circular buffers. The data in the circular buffers is processed on board the PSC for out of tolerance conditions and transmitted to the main NSLS II control system. The PSC has sufficient on board memory to store multiple ramps and numerous monitoring buffers. There is one PSC for each PSI. The PSC cards are grouped in chassis. There can be up to twenty PSC cards in one chassis. The data transfer frequency between the PSC and PSI is 10 KHz. The PSC will receive trigger signals from an Event Receiver module located in the IOC chassis. These triggers will be used to synchronize the starts of current ramps of the booster power supplies. The Cell Controller communicates with the PSC chassis through a dedicated network. The Cell Controller communicates with an EPICS based IOC through standard high speed Ethernet. The EPIC IOC will have high level programming tools to control the power supplies and generate current ramps.

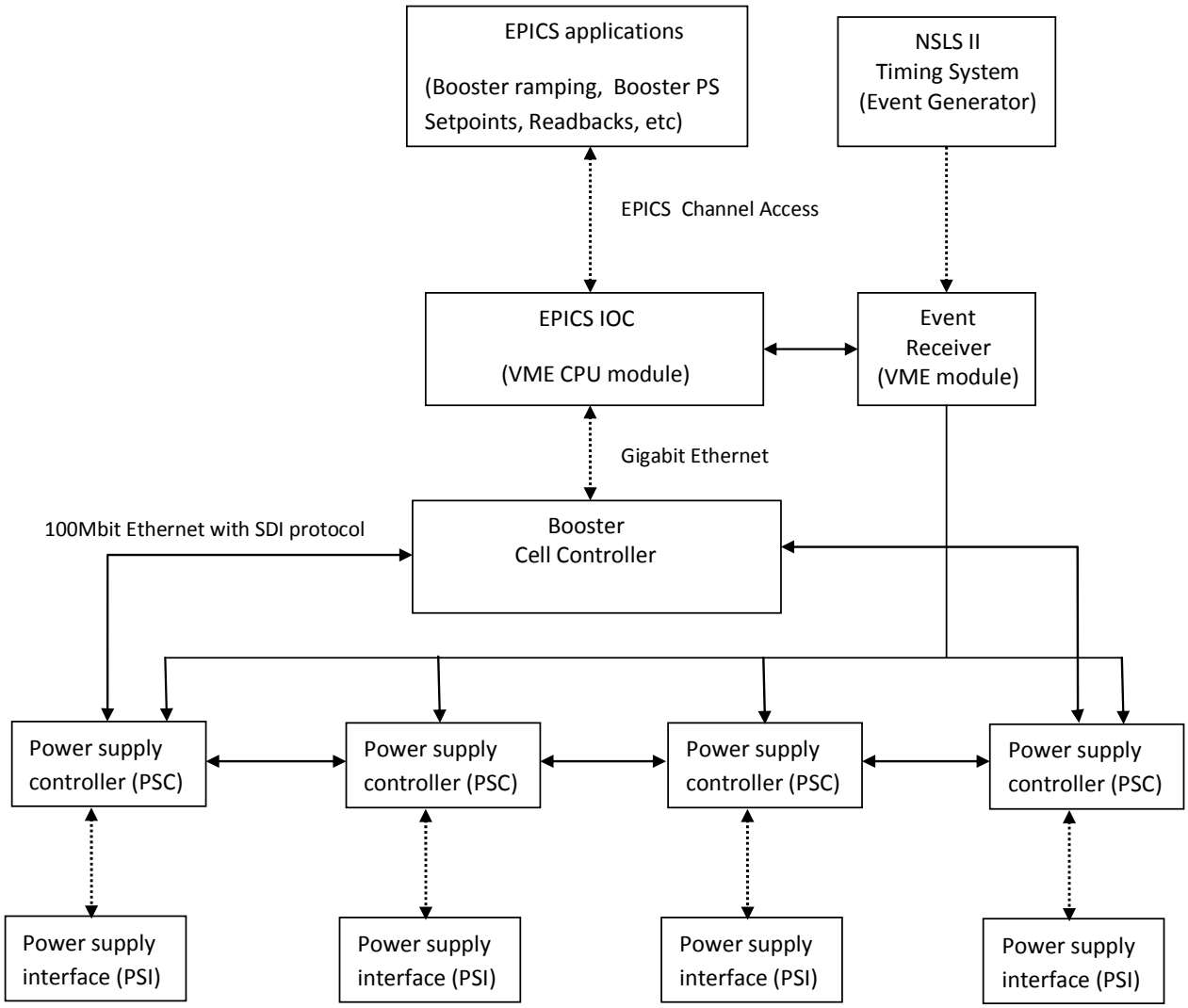

Figure 27: Booster Power Supply Control Scheme

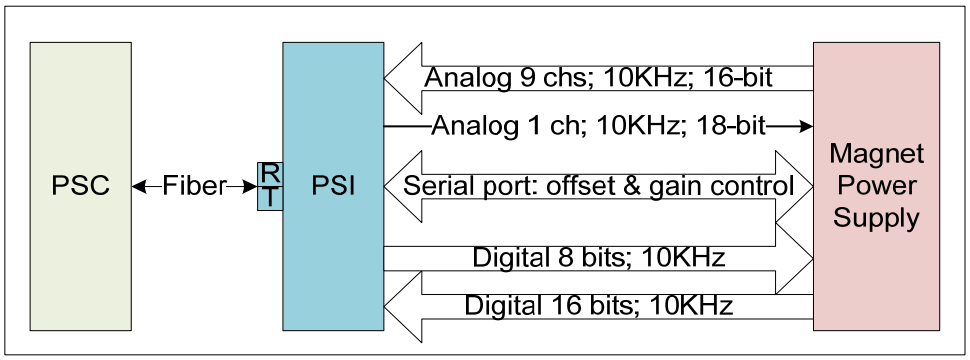

Figure 28: PSI Functional Block Diagram

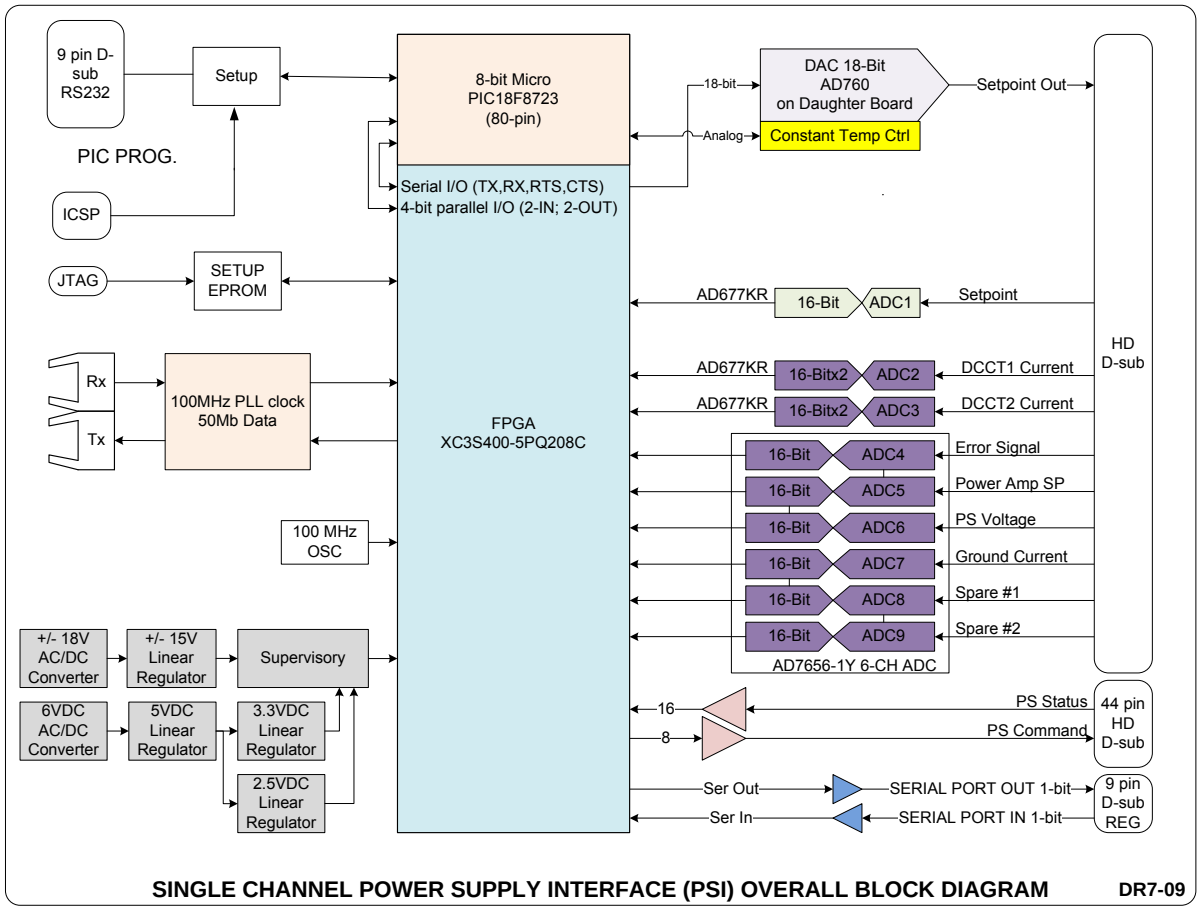

Figure 29: PSI Block Diagram

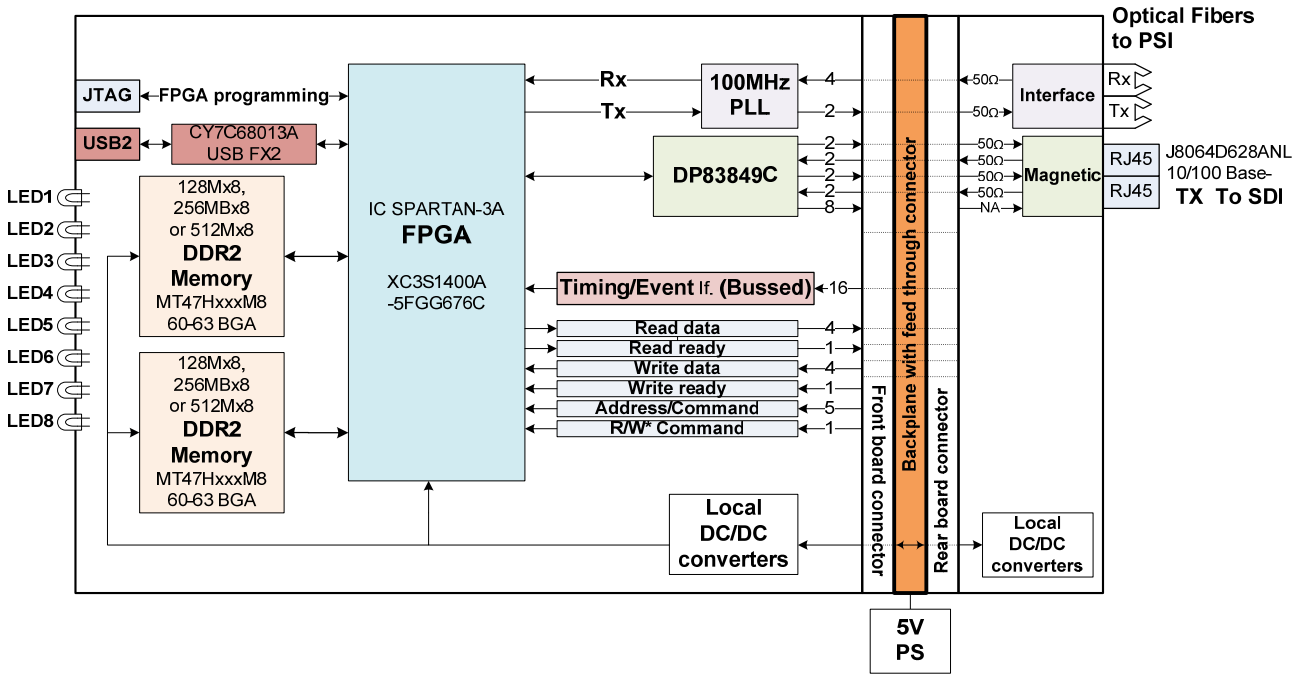

Figure 30: PSC Block Diagram

Electrical Utilities

Equipment Racks

All booster ring rack mountable equipment will be installed in sealed NEMA 12 equipment racks. The racks will be assembled in either 2, 3, 4, 5 rack groups. The A water-to-air heat exchanger will cool a rack group in a closed cycle. Cooled air will flow through the equipment mounted in the rack, and circulate back to the heat exchanger. Air circulation is to be from the front of the rack to the rear through the equipment. Cooled air shall be ducted to the space between the front door and the front panel. Heated air will be collected in the top of the racks and ducted to the heat exchangers mounted in the side of the rack group. The heat exchanger will use chilled water and have the air outlet temperature regulated to 24 $\pm$ 1 ° C. The chilled water to air heat exchanges are mounted on the sides of the rack groups. The nominal cooling capacity for each rack is 5000 watts. The two rack group will use two heat exchangers mounted on a single side and the three, four, and five rack group will have heat exchangers mounted on both sides (Fig. 28). Cables entering the racks will go through entry seals located at the top of the rack. All the rack groups will have temperature monitoring and smoke alarms that will be connected to the NSLS II control system.

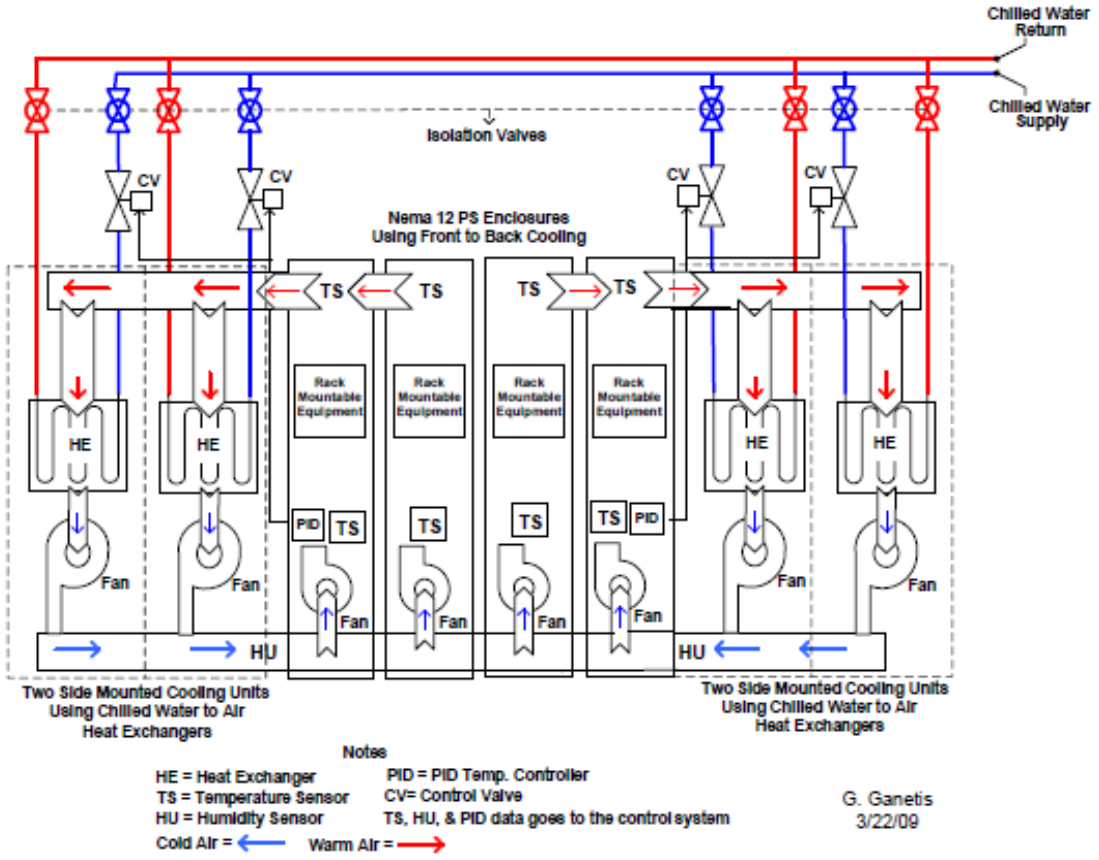

Figure 31: Rack Cooling Scheme

Cabling

Power cables will be arranged to minimize pickup to other circuits in the booster and/or storage ring. The cables for the magnet powering circuits will be configured to eliminate any large loops. Cable trays will be mounted on the side of the booster magnet girder for magnet circuits and instrumentation. The cable trays will use a multi-segment tray assemblies. Each segment will contain a different cable classification to segregate different voltage level and functions. All cable used will be rated for use in a cable tray and will meet all regulatory requirement (NEC & OSHA). The tray and grounding cables located in the tray will also be configured to eliminate any large area ground loops.

11 Control System

All parameters essential for the operation of the booster according to specification shall be monitored and controlled by the booster control system. The booster control system is an integral part of the NSLS-II accelerator control system. To minimize long-term costs of maintenance for software and equipment, it will be built using all NSLS-II standards.

The NSLS-II standards include (fig. 32): use of EPICS for mid level control, use of industrial PCs running VxWorks for front-end computers, and the use of PMC and PCI for I/O. An Ethernet interface from the Industrial

PC to Allen-Bradley Control Logix PLC I/O and its related field I/O shall be used for slow, widely distributed, and slow equipment protection. VME I/O that is integrated through a PCI to VME bridge may be used when the density or I/O type requires it.

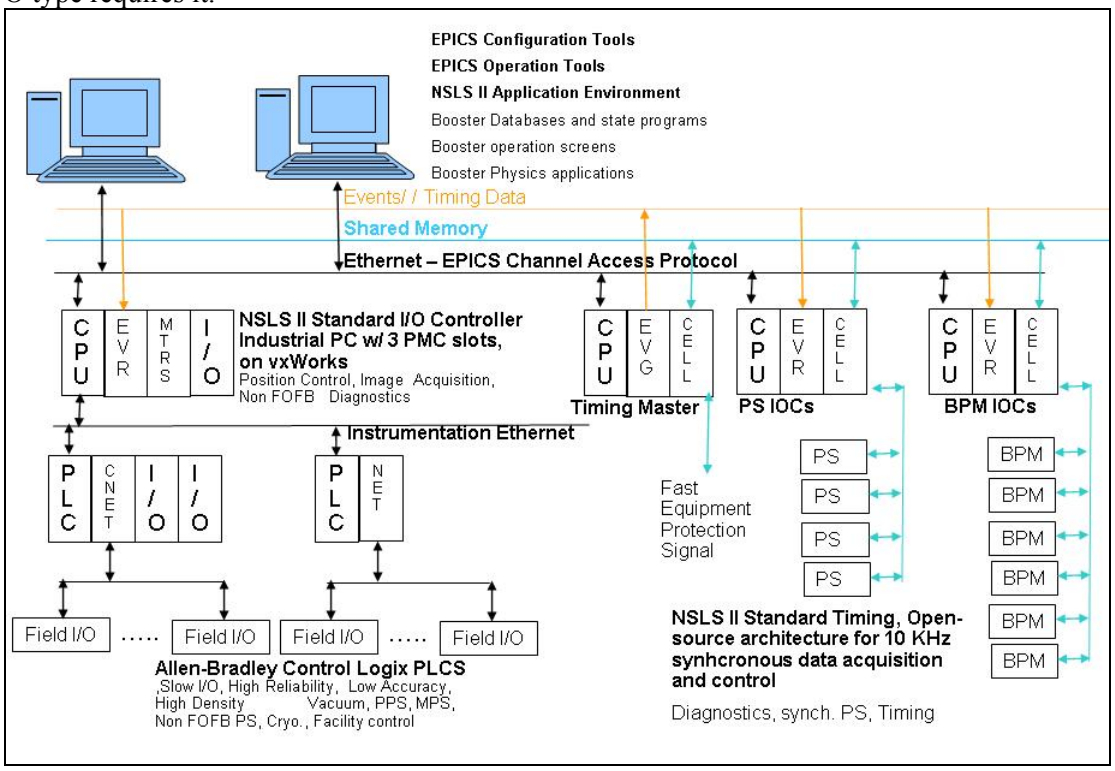

Figure 32: Architecture of the NSLS-II control system

NSLS-II injector naming standard is established and controlled. All injector subsystems will include Piping and Instrumentation Diagram type displays that show the current state of the subsystem components. All signals monitored or internal to any device controllers will be provided to the control system. Any communication protocols will provide statistics and information on the health of the communication over that protocol.

The timing system for the NSLS-II will use the Micro Research Oy hardware suite for event generators, event receivers and fiber optic distribution. Detailed information can be obtained from the Micro Research web site at: http://www.mrf.fi/index.php?option=com_frontpage&Itemid=1

A brief description of the system topology follows below.

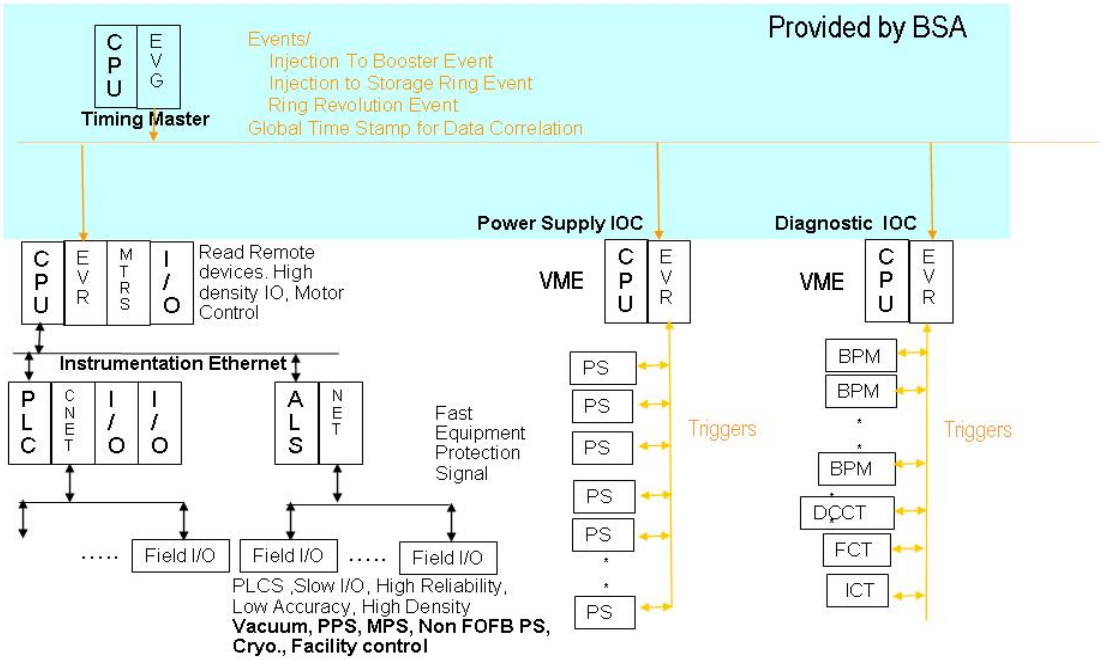

The timing system is a distributed system with an event generator (EVG), distributing time stamps and events throughout the facility to the event receivers (EVR). Each event receiver can produce triggers relative to any of the global events. In addition to the distribution of events, the EVG sends a time stamp to each IOC. The IOC uses this time stamp to identify data throughout the control network so that data correlation is possible. Each IOC should have an Event Receiver to provide this time stamp. In the Booster contract, the EVG, and fanouts, and fiber up to the EVRs is provided by BSA.

12 Injection System Service Building

In the following we briefly describe the injector service building layout (Figure 33). The service area will contain all injector equipment including that for the linac, transport lines and booster. It will also include rooms for utility distribution system, workbenches and local control room. Equipment for the injection straight in the storage room will be located on the mezzanine above the straight section.

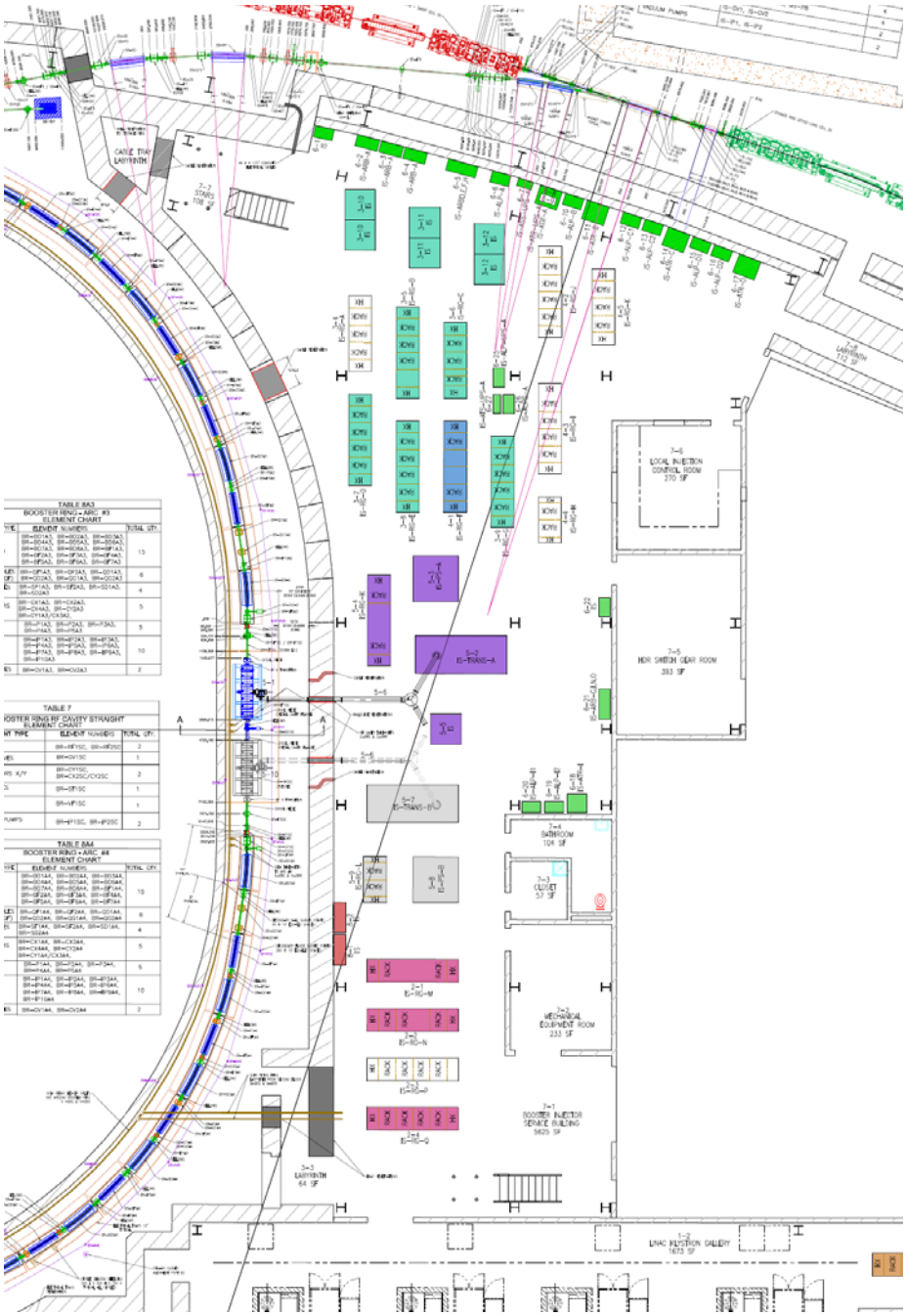

Figure 33: Layout of the injector service area

Areas in the injector service building are included in the list below.

1. Injector building areas

TABLE 5A

REGION	DESCRIPTION	QTY
1–1	LINAC BUILDING	1
1–2	LINAC KLYSTRON GALLERY	1
1–3	LINAC LABYRINTH	1
1–4	LINAC LABYRINTH	1
1–5	LINAC RACKS (4)	1
1–6	–	–
1–7	–	–
1–8	–	–
1–9	–	–
1–10	–	–
2–1	LBTL CORR & SPARE POWER SUPPLIES & HEAT EXCHANGERS (SPARE)	1
2–2	LBTL DIPOLE, QUAD, & CORR POWER SUPPLIES & HEAT EXCHANGERS	1
2–3	LBTL VACUUM & DIAGNOSTICS & HEAT EXCHANGERS	1
2–4	LINAC, LTB DIAGNOSTICS (3 RACKS)	1
2–5		
2–6	–	–
2–7	–	–
2–8	–	–
2–9	–	–
2–10	–	–
2–11	–	–
3–1	BOOSTER RING TUNNEL	1
3–2	BOOSTER RING LABYRINTH	1
3–3	BOOSTER RING LABYRINTH	1
3–4	BOOSTER DIAGNOSTICS (2 RACKS)	1
3–5	BOOSTER CORR. POWER SUPPLIES & HEAT EXCHANGERS	1
3–6	BOOSTER QUAD. POWER SUPPLIES & HEAT EXCHANGERS	1
3–7	BOOSTER DIAGNOSTICS (2 RACKS)	
3–8	BOOSTER VACUUM DIAGNOSTICS & HEAT EXCHANGERS	1
3–9	BOOSTER SPARE RACK SPACE & HEAT EXCHANGERS (SPARE)	1
3–10	BOOSTER BD1 POWER SUPPLY CABINET	2
3–11	BOOSTER BD2 POWER SUPPLY CABINET	2
3–12	BOOSTER BF POWER SUPPLY CABINET	2
3–13	–	–
3–14	–	–
	–	
	–	
	–	–
	–	–
3–19	–	–
3–20	–	–
4–1	BSRTL VACUUM & DIAGNOSTICS & HEAT EXCHANGERS	–
4–2	BSRTL DIPOLE,QUAD & CORR POWER SUPPLIES & HEAT EXCHANGERS	–
4–3	BSRTL CORR & SPARE POWER SUPPLIES & HEAT EXCHANGERS (SPARE)	1
4–4	INJECTION SYSTEM TIMING & HEAT EXCHANGERS	1
4–5	BSRTL SPARE RACK SPACE & HEAT EXCHANGERS (SPARE)	1
4–6	–	–
4–7	–	–
4–8	–	–
4–9	–	–
4–10	–	–
5–1	BOOSTER 7 CELL RF CAVITY	1
5–2	BOOSTER RF TRANSMITTER A CABINET	1
5–3	BOOSTER RF HIGH VOLTAGE POWER SUPPLY A CABINET	1
5–4	BOOSTER RF CONTROLS & HEAT EXCHANGERS	1
5–5	BOOSTER RF WATER COOLED TEST LOAD	1
5–6	WAVEGUIDE	1
5–7	BOOSTER RF TRANSMITTER B CABINET (FUTURE)	1
5–8	BOOSTER RF HIGH VOLTAGE POWER SUPPLY B CABINET (FUTURE)	1
5–9	BOOSTER SPARE RACK & HEAT EXCHANGERS (FUTURE)	1
5–10	BOOSTER 7 CELL RF CAVITY (FUTURE)	1

TABLE 5B

REGION	DESCRIPTION	QTY
6–1	460 REMOTE OPERATION	1
6–2	480 CB	1
6–3	480 CB	1
6–4	480 CB	1
6–5	480 LP	1
6–6	208 LP	1
6–7	SAFETY SWITCH	1
6–8	115KVA TRANSFORMER	1
6–9	45 KVA TRANSFORMER	1
6–10	208 LP	1
6–11	115 KVA TRANSFORMER	1
6–12	208 LP	1
6–13	208 LP	1
6–14	115 KVA TRANSFORMER	1
6–15	208 LP	1
6–16	208 LP	1
6–17	115 KVA TRANSFORMER	1
6–18	115 KVA TRANSFORMER	1
6–19	208 LP	1
6–20	208 LP	1
6–21	460 LP	1
6–22	460 REMOTE OPERATION	1
6–23	TRANSFER SWITCH	1
6–24	UPS	1
6–25	208 LP	1
6–26	–	–
6–27	–	–
6–28	–	–
6–29	–	–
6–30	–	–
7–1	BOOSTER INJECTOR SERVICE BUILDING	1
7–2	MECHANICAL EQUIPMENT ROOM	1
7–3	CLOSET	1
7–4	BATHROOM	1
7–5	HDR SWITCH GEAR ROOM	1
7–6	LOCAL INJECTION CONTROL ROOM	1
7–7	STAIRS	1
7–8	LABYRINTH	1
7–9	–	
7–10	–	–
8–1	PPS CABINET A	1
8–2	PPS–CABINET B	1
8–3	–	–
8–4	–	–
8–5	–	–
8–6	–	–
8–7	–	–
8–8	–	–
8–9	–	–
8–10		–

13 Booster Supplementary Shielding

The theoretical analysis of the required shielding around the NSLS 2 Booster Ring is presented Preliminary Design Report under ESH & Q, Chapter 2: Radiation Safety and Shielding [14]. Consequently, the mechanical design of the necessary supplemental shielding around the Booster Ring was based on that background analysis.

This section focuses mainly on the mechanical aspects of the shielding for the (1) Booster Beam Dump, (2) Booster Injection/Extraction components, and (3) shadow shielding required due to the radiation emanating from the Booster Ring dipole magnets.

Booster Beam Dump

The Beam Dump will be made of 10-cm. dia by 35 cm long solid iron cylinder, encased with 15 cm. thick lead and surrounded by an additional 20 cm thick Polyethelyne for neutron shielding. For simplicity and to minimize cost, the dump will be supported directly from the floor by a pile of concrete bricks. Fig. 31 shows the iron dump with the top half of the lead and poly enclosure removed.

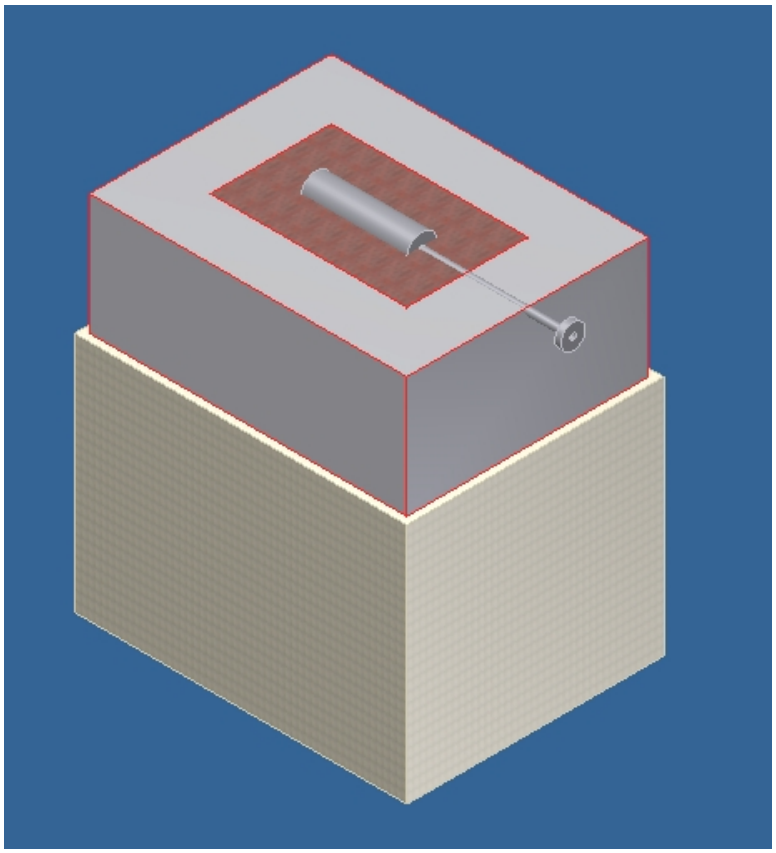

Figure 34: Booster Beam Dump

Booster Extraction and Injection Septa

The Booster Extraction and Injection Septa will be protected with lead shielding on 3 sides; the only side that is left unshielded is the side directly facing the tunnel floor. Since there is no available headroom in the Booster Ring to suspend the shielding from the ceiling, it has to be supported from the tunnel floor.

The lead shielding enclosure shall be designed such that at least one side will be conveniently movable in order to allow access to the septum magnet whenever necessary. This movable side shall be equipped with a drive mechanism to lower it down in order to allow quick access to the septum. The roof shielding and the other side of the lead enclosure can be erected as a semi-permanent structure that can be dismantled manually if need be.

The lead shielding shall be located as close as possible to the radiation source. The required lead thickness is only 15 cm, but enough space should be allocated to allow for the structural framework and drive. There should be also adequate space underneath the septum girder to allow tie bars from one side to the other in order to make the shielding structure solid and rigid. Fig. 32 shows the foot print and the required dimensions.

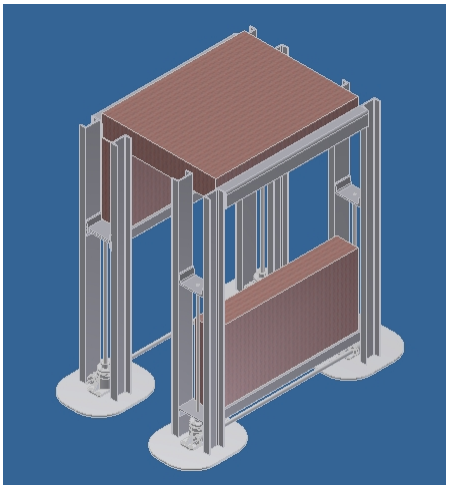

Fig. 35a: Septum Shield (Vertical Shields Movable)

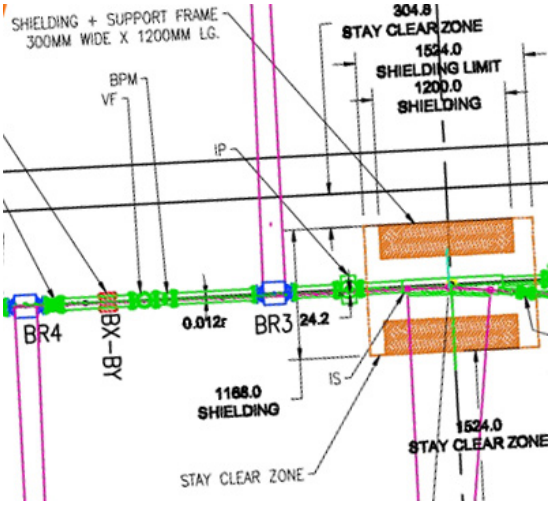

Fig. 35b: Injection Septum Shield Footprint

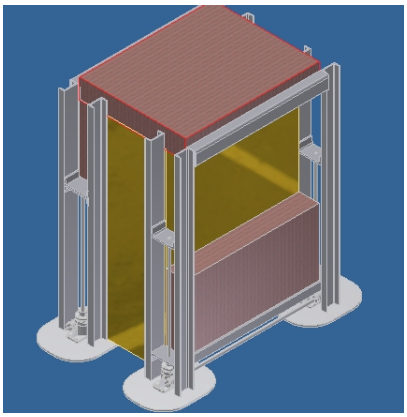

Fig. 35c: Septum Shield (Septum Envelope Shown)

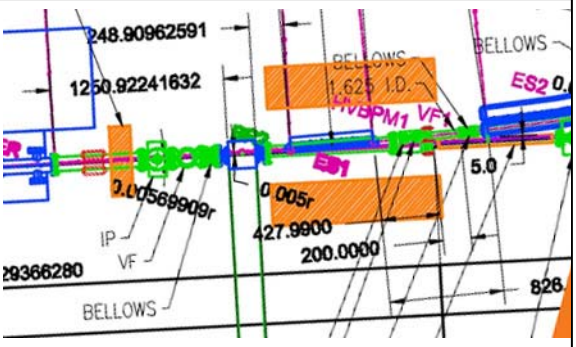

Fig. 35d: Extraction Septum Shield Footprint

Booster Dipole Magnets Shadow Shields

There will be "shadow" lead shielding on some Booster Ring magnets, each with 20 cm x 20 cm x 15 cm thick and positioned at 20 locations around the Booster Ring as indicated in the general Booster Ring drawing. Each shield will be mounted separately on pedestal-type stands anchored to the floor as shown on Fig. 36 below.

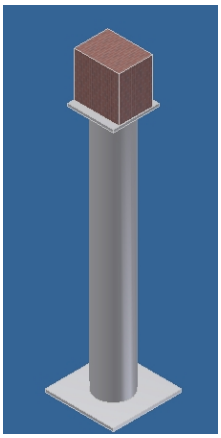

Fig. 16a: Shield on Pedestal

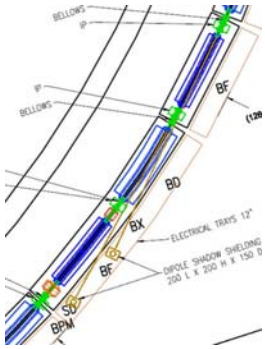

Fig. 36b: Typical Footprint of Shadow Shields

References

[1] http://ieeexplore.ieee.org/iel5/10603/33511/01591747.pdf?arnumber=1591747 asp
[2] http://accelconf.web.cern.ch/AccelConf/e02/PAPERS/TUPRI097.pdf
[3] http://ieeexplore.ieee.org/iel5/10603/33511/01591041.pdf?arnumber=1591041
[4] The SLS booster synchrotron, W. Joho, M. Muñoz and A. Streun, Nucl. Instrum. and Meth. A**,** Vol. 562-1, pp. 1-11
[5] http://epaper.kek.jp/e06/PAPERS/THPLS057.PDF
[6] http://ieeexplore.ieee.org/iel5/10603/33511/01590651.pdf?arnumber=1590651
[7] I. Pinayev, et.al. "Injection Simulations for the NSLS-II Storage Ring". Proceedings of the Particle Accelerator Conference 2007, Albuquerque, NM. TUPMS077.
[8] M. Munoz and V. Joho, Eddy current effects in the SLS booster: http://**sls**bd.psi.ch/pub/**sls**notes/tmeta9810/**eddy**.html
[9] http://www.i-tech.si/products.php
[10] http://www.bergoz.com/products/NPCT/PCT-downloads/files/NPCTflyer.pdf
[11] http://www.bergoz.com/products/FCT/d-fct.html
[12] http://www.optronis.com/
[13] T. Shaftan, R. Heese and N. Tsoupas, NSLS-II Tech. note-2008
[14] http://www.bnl.gov/nsls2/project/PDR/4-ESHQ_Ch_2_Rad_Safety.pdf

Appendix A

Booster lattice in MAD format

```
! NSLS-II booster lattice NSLS2blat4-3.txt
ABD=0.1464522526788075
ABF=0.05702547219491924
ABD2=ABD/2
ABF2=ABF/2
RF :RFCAVITY,L=0.000001,VOLT=1.2,HARMON=264
BD: SBEND,L=1.3,ANGLE=ABD,K1=-5.550893E-01, &
E1=ABD2,E2=ABD2, K2=-4.3*1
BF: SBEND,L=1.24,ANGLE=ABF,K1=8.20000E-01, &
E1=ABF2,E2=ABF2, K2=3.6*1
D1: DRIFT,L=0.51
D2: DRIFT,L=0.51
D2a: DRIFT,L=0.25
DA: DRIFT,L=3.31
DEX: DRIFT,L=1.0
DEX3: DRIFT,L=0.3333333
DB: DRIFT,L=0.4
DC: DRIFT,L=0.75
DD: DRIFT,L=0.25
DE: DRIFT,L=0.53
DG: DRIFT,L=0.61
DSE: DRIF,L=0.225
MK1: MARKER
MK2: MARKER
MBX: MARKER
MON: Moni, L=0.000001
BX: HKICKer,L=0.000001,KICK=1E-9
BY: VKICKer, L=0.000001, KICK=1E-9
QD: QUAD,L=0.2,K1=-1.359655
QF: QUAD,L=0.3,K1=1.95
QG: QUAD,L=0.2,K1=1.433046
SF: SEXT,L=0.15,K2=0.0
SD: SEXT,L=0.15,K2=0.0
SSF: LINE=(DSE,SF,DSE)
SSD: LINE=(DSE,SD,DSE)
CL: LINE=(BD,D1,BF,D2)
CQ: LINE=(QG,DG)

DSL: LINE=(DA,MON,BX,BY,DEX,QF,DB,BD,DC,CQ,QD,DD,BF,DE,BX)
DSR: LINE=(MON,DE,BF,DD,QD,-CQ,DC,BX,BD,DB,QF,DEX,BY,DA)
ARC: LINE=(BD,MON,SSF,BF,D2a,BX,D2a,BD,MON,SSD,BF,D2a, &
BY,D2a,CL,BD,D2a,BX,D2a,BF, &
SSD,MON,BD,D2a,BY,D2a,BF,SSF,MON,BD)
ARC2: LINE=(BD,MON,SSF,BF,D2a,BX,D2a,BD,SSD,MON,BF,D2a, &
BY,D2a,BD,D1,BF2)

ARC2R: LINE=(-ARC2)
PER: LINE=(MK1,DSL,ARC,DSR,MK2)
PER2: LINE=(MK1,DSL,ARC2,-ARC2,-DSL,MK2)
PER3: LINE=(-ARC2,-DSL,MK2)
RING: LINE=(4*PER, RF)
```